α-synuclein BAC transgenic mice exhibited RBD-like behavior and hyposmia: A prodromal Parkinson's disease model

Tomoyuki Taguchi, M.D.[1, *], Masashi Ikuno, M.D.[1,*], Mari Hondo, Ph.D.[2], Laxmi Kumar Parajuli, PhD[3], Katsutoshi Taguchi, Ph.D.[4], Jun Ueda, M.D.[1], Masanori Sawamura, M.D.[1], Shinya Okuda, M.D.[1], Etsuro Nakanishi, M.D.[1], Junko Hara, Ph.D.[1], Norihito Uemura, M.D., Ph.D.[1], Yusuke Hatanaka, Ph.D.[1], Takashi Ayaki, M.D. Ph.D.[1], Shuichi Matsuzawa, Ph.D.[1], Masaki Tanaka, M.D., Ph.D.[4], Omar M.A. El-Agnaf, Ph.D. [5], Masato Koike, M.D., Ph.D.[3], Masashi Yanagisawa, M.D., Ph.D.[2], Maiko T. Uemura, M.D. Ph.D.[1, #] , Hodaka Yamakado, M.D., Ph.D.[1, #], Ryosuke Takahashi, M.D., Ph.D.[1, #]

[1] Department of Neurology Kyoto University Graduate School of Medicine, Kyoto, Japan.

[2] International Institute for Integrative Sleep Medicine (WPI-IIIS), The University of Tsukuba, Ibaraki, Japan.

[3] Department of Cell Biology and Neuroscience, Juntendo University Graduate School of Medicine, Tokyo, Japan.

[4] Department of Anatomy and Neurobiology, Graduate School of Medical Science, Kyoto Prefectural University of Medicine, Kyoto, Japan.

[5] Neurological Disorders Research Center, Qatar Biomedical Research Institute (QBRI), Hamad Bin Khalifa University (HBKU), Qatar Foundation, Doha, Qatar.

* First and second author contributed equally.

Corresponding to:

Hodaka Yamakado, MD, PhD

Department of Neurology, Kyoto University Graduate School of Medicine

54 Shogoin Kawahara-cho, Sakyo-ku, Kyoto 606-8507 Japan

TEL: +81-75-751-3767

FAX: +81-75-761-9780

E-mail address: yamakado@kuhp.kyoto-u.ac.jp

Maiko T. Uemura, MD, PhD

Department of Neurology, Kyoto University Graduate School of Medicine

54 Shogoin Kawahara-cho, Sakyo-ku, Kyoto 606-8507 Japan

TEL: +81-75-751-3767

FAX: +81-75-751-9541

E-mail address: maikohs@kuhp.kyoto-u.ac.jp

Ryosuke Takahashi, MD, PhD

Department of Neurology, Kyoto University Graduate School of Medicine

54 Shogoin Kawahara-cho, Sakyo-ku, Kyoto 606-8507 Japan

TEL: +81-75-751-4397

FAX: +81-75-761-9780

E-mail address: ryosuket@kuhp.kyoto-u.ac.jp

Short running title:

α-synuclein BAC Tg mice model for prodromal PD

Abstract

Parkinson's disease is one of the most common movement disorders and is characterized by dopaminergic (DA) cell loss and the accumulation of pathological α-synuclein (α-syn), but its precise pathogenetic mechanisms remain elusive. To develop disease-modifying therapies for Parkinson's disease, an animal model that recapitulates the pathology and symptoms of the disease, especially in the prodromal stage, is indispensable. Since subjects with α-syn gene (*SNCA*) multiplication as well as point mutations develop familial Parkinson's disease and a genome-wide association study (GWAS) in Parkinson's disease has identified *SNCA* as a risk gene for Parkinson's disease, the increased expression of α-syn is closely associated with the etiology of Parkinson's disease. In this study we generated bacterial artificial chromosome (BAC) transgenic mice harboring *SNCA* and its gene expression regulatory regions in order to maintain the native expression pattern of α-syn. Furthermore, in order to enhance the pathological properties of α-syn, we inserted into *SNCA* an A53T mutation, two single-nucleotide polymorphisms identified in a GWAS in Parkinson's disease and a Rep1 polymorphism, all of which are causal of familial Parkinson's disease or increase the risk of sporadic Parkinson's disease. These A53T *SNCA* BAC transgenic mice showed an expression pattern of human α-syn very similar to that of endogenous mouse α-syn. They expressed

truncated, oligomeric and proteinase K-resistant phosphorylated forms of α-syn in the regions that are specifically affected in Parkinson's disease and/or dementia with Lewy bodies, including the olfactory bulb, cerebral cortex, striatum and substantia nigra. Surprisingly, these mice exhibited rapid eye movement (REM) sleep without atonia, which is a key feature of REM sleep behavior disorder (RBD), at as early as five months of age. Consistent with this observation, the REM sleep-regulating neuronal populations in the lower brainstem, including the sublaterodorsal tegmental nucleus, nuclei in the ventromedial medullary reticular formation and the pedunculopontine nuclei, expressed phosphorylated α-syn. In addition, they also showed hyposmia at nine months of age, which is consistent with the significant accumulation of phosphorylated α-syn in the olfactory bulb. The DA neurons in the substantia nigra pars compacta degenerated, and their number was decreased in an age-dependent manner by up to 17.1% at 18 months of age compared to wild-type, although the mice did not show any related locomotor dysfunction. In conclusion, we created a novel mouse model of prodromal Parkinson's disease that showed RBD-like behavior and hyposmia without motor symptoms.

Keywords

Parkinson's disease; alpha-synuclein; RBD; hyposmia; prodromal PD

Abbreviation list

ANOVA: analysis of variance

α-syn: α-synuclein

BAC: bacterial artificial chromosome

BAC-*SNCA*$^{A53T/-}$: heterozygous A53T BAC-*SNCA* transgenic

BAC-*SNCA*$^{A53T/A53T}$: homozygous A53T BAC-*SNCA* transgenic

BCA: Bicinchoninic Acid

DA: dopaminergic

DAT: dopamine transporter

DLB: dementia with Lewy bodies

DMN: dorsal motor nucleus of vagus nerve

DMT: disease-modifying therapy

EDTA: ethylenediaminetetraacetic acid

EEG: electroencephalography

EMG: electromyography

GiA: alpha gigantocellular nucleus

GiV: ventral gigantocellular nucleus

GWAS: genome-wide association study

NREM: non-REM

PAC: P1-derived artificial chromosome

PAGE: poly acrylamide gel electrophoresis

p-α-syn: phosphorylated α-syn

PBS: phosphate buffered saline

PCR: Polymerase chain reaction

PFA: paraformaldehyde

PK: proteinase K

PPN: pedunculopontine tegmental nucleus

PSG: polysomnography

PVDF: polyvinylidene difluoride

RBD: rapid eye movement sleep behavior disorder

RMg: raphe magnus

RSWA: rapid eye movement sleep without atonia

SDS: sodium dodecyl sulfate

SLD: sublaterodorsal tegmental nucleus

SNc: substantia nigra pars compacta

SNcd: substantia nigra pars compacta, dorsal part

SNcl: substantia nigra pars compacta, lateral part

SNcm: substantia nigra pars compacta, medial part

SNcv: substantia nigra pars compacta, ventral part

SNPs: single nucleotide polymorphisms

TH: tyrosine hydroxylase

VTA: ventral tegmental area

VMRF: ventromedial medullary reticular formation

Introduction

Parkinson's disease is the most common neurodegenerative movement disorder and is characterized by motor symptoms, including bradykinesia, rigidity, tremor and postural instability, as well as a variety of non-motor symptoms, such as hyposmia, sleep disorders, psychiatric symptoms and dysautonomia (Poewe *et al.*, 2017; Schapira *et al.*, 2017). Among non-motor symptoms, which frequently antedate motor symptoms by several years or more, hyposmia and polysomnography (PSG)-proven rapid eye movement sleep behavior disorder (RBD) have high positive likelihood ratios of 4.0 and 130, respectively, for the development of Parkinson's disease (Berg *et al.*, 2015). The prodromal stage of Parkinson's disease provides an excellent opportunity to understand the very early changes associated with the disease and to start disease-modifying therapies (DMTs) that may delay the disease progression and subsequent development of motor symptoms. From this perspective, animal models that recapitulate the symptoms and pathologies of Parkinson's disease, especially in the prodromal stage, are urgently needed.

The pathological hallmarks of sporadic Parkinson's disease are the loss of dopaminergic (DA) neurons in the substantia nigra pars compacta (SNc) in association with Lewy bodies and Lewy neurites, both of which are mainly composed of aggregated α-synuclein

(α-syn) (Spillantini *et al.*, 1997, 1998). The central role of α-syn in Parkinson's disease has been established by several lines of evidence: 1) point mutations and multiplications in *SNCA*, the gene encoding α-syn, cause familial Parkinson's disease (Chartier-Harlin *et al.*, 2001; Olgiati *et al.*, 2015); 2) a genome-wide association study (GWAS) in Parkinson's disease identified risk-associated single nucleotide polymorphisms (SNPs) in *SNCA*, and these risk-associated SNPs increase the α-syn gene expression; 3) α-syn is the major constituent of Lewy pathology in the brain and peripheral nervous systems (Spillantini *et al.*, 1997); 4) the overexpression of α-syn shows neurotoxic effects *in vitro* and *in vivo* (Baekelandt *et al.*, 2002; Kirik *et al.*, 2002; Macchi *et al.*, 2016); and 5) the inoculation of α-syn fibrils causes α-syn aggregate propagation and the progressive loss of DA neurons (Luk *et al.*, 2012; Masuda-Suzukake *et al.*, 2013). These lines of evidence have paved the way for the development of α-syn–based animal models that replicate key pathological features of the disease (Visanji *et al.*, 2016).

Regarding genetic animal models, a number of α-syn–based transgenic animal models have been generated. Several mice models reproduced the α-syn aggregation and toxicity *in vivo* and have greatly contributed to our understanding of the disease (Fleming *et al*., 2008, Giasson *et al*., 2002). However, most of these models do not develop DA cell loss nor show

motor/non-motor symptoms of Parkinson's disease faithfully, probably due to the ectopic overexpression of α-syn by the exogenous promoters. As such, genome-based bacterial artificial chromosome (BAC) transgenic mice expressing target proteins under the control of the native promoter and gene expression regulatory regions seem useful for producing more accurate genetic models. There were various types of BAC/P1-derived artificial chromosome (PAC)-*SNCA* mice models reported and some of them showed systemic α-synucleinopathy, motor dysfunction, hyposmia or vulnerability to drugs (Kuo *et al.,* 2010; Yamakado *et al*., 2012; Hansen *et al*., 2013; Janezic *et all,* 2013; Cannon *et al.,* 2013; Taylor *et al.,* 2014; Cronin *et al.,* 2009). They brought important findings such as native distribution of α-syn and its effect on behaviors. However, there were no mice models which showed age-related chronic and selective DA degeneration coupled with multiple prodromal symptoms. Unlike mice models, BAC-*SNCA* rat model was reported to show tyrosine-hydroxylase (TH)- positive cell loss and hyposmia (Nuber *et al.*, 2013). However, mice model has advantage in handling and genetic engineering. Moreover, there are no animal model which showed RBD phenotypes as a prodromal symptom in Parkinson's disease. We previously generated BAC-*SNCA* transgenic mice harboring the entire wild-type human *SNCA* and its gene expression regulatory regions (Yamakado *et al.*, 2012). The mice showed a native expression pattern of human α-syn and

decreased anxiety-like behaviors but did not recapitulate the pathological changes of Parkinson's disease, including DA cell loss and α-syn aggregation. To enhance the pathological property of α-syn, we inserted an A53T point mutation, which is the causative gene mutation of familial Parkinson's disease and known to facilitate α-syn aggregation, into the BAC-*SNCA* transgenic construct (Conway *et al.*, 2000; Rodriguez *et al.*, 2015). Parkinson's disease patients with A53T mutation showed similar but accelerated phenotype of idiopathic Parkinson's disease in terms of the distribution of Lewy pathology and associated prodromal non-motor symptoms (Spira *et al.,* 2001). In addition, we also introduced two risk-associated SNPs (rs11931074 and rs3857059) and an Rep1 dinucleotide repeat polymorphism into the *SNCA* promoter region (259 to 261 alleles), all of which increase the risk of developing sporadic Parkinson's disease (Maraganore *et al.*, 2006; Satake *et al.*, 2009; Han *et al.*, 2015). The majority of people have these risk variants, but as the original BAC construct has minor protective polymorphisms (Kenneth *et al.*, 2009; Maraganore *et al.,* 2006*;* Satake *et al.,* 2009), we edited the construct in order to introduce major alleles and eliminate minor protective factors.

We therefore analyzed the pathological phenotypes and Parkinson's disease-related motor as well as non-motor symptoms in this model.

Materials and methods

Animals

All mice used in this study were handled in accordance with the national guidelines. The mice were maintained at 25 °C with 55% humidity on a 12-h light-dark cycle and given free access to food and drinking water. All procedures performed in this study were approved by the Institutional Animal Care and Use Committee, Institute of Laboratory Animals Graduate School of Medicine, Kyoto University (170274) and the University of Tsukuba Animal Care and Use Committee.

A53T BAC-*SNCA* transgenic mice were generated as previously described (Yamakado *et al.*, 2012) with some modification. In brief, A53T, rs11931074 (G to T) and rs3857059 (A to G) mutations as well as Rep1 copy number variation (259 to 261) were introduced into human α-syn BAC construct using the Red/ET recombination system (K002, Counter-Selection BAC Modification Kit; Gene Bridges, Heidelberg, Germany). The construct consists of P1-derived artificial chromosome (PAC) AF163864 and BAC AC09748 and contains 28-kb 5'- and 50-kb 3'-flanking regions in addition to the entire human *SNCA* (Yamakado *et al.*, 2012) (Fig. 1A). The resultant vector was injected into the fertilized eggs of C57BL/6J mice. Polymerase chain reaction (PCR) was performed with the following primer set: *SNCA* fw 5'-

ACTTGCTAGGCCACCTGAGA-3', *SNCA* rv 5'-ATGCCAGGTGTTTGGAAAAG-3, followed by electrophoresis on a 2% (*w*/*v*) agarose gel. Real-time PCR for *SNCA* and *IL2*, a reference gene, were performed with the following primer sets: *SNCA* fw: 5'-GGCTGATGCCAACAAGCTGT-3', *SNCA* rw: 5'-GTGGAATTTCGCACAAACCCT-3'; *IL2* fw: 5'-ATAAATTGCCTCCCATGCTGA-3', *IL2* rv: 5' -GATGCGAGCTGCATGCTGTA-3'.

Immunohistochemical and electron microscopic analyses

Described in the supplementary materials.

Cell counting

The number of DA neurons in the SNc was quantified as previously described (Luk *et al.*, 2012; Tran *et al.*, 2014) with minor modification. The images of every 10th section of TH-immunostained coronal sections through the entire midbrain were captured with a microscope (BX43; OLYMPUS, Tokyo, Japan). Immunoreactive neurons were counted at 10 × magnification following previously described criteria for each subgroup (SNcd: dorsal part, SNcm: medial part, SNcv: ventral part and SNcl: lateral part) (Fu *et al.*, 2012). The number of intact neurons with visible nuclei was counted.

Sequential extraction

For biochemical analyses, phosphate-buffered saline (PBS)-perfused mouse brains (3, 9, and 18 months; n = 6, respectively) and human frontal cortices (the information of human brain samples is listed in supplementary table 1) were homogenized in 10 volume of 1% triton lysis buffer (10 mM Tris·HCl [pH 7.4], 150 mM NaCl, 1 mM ethylenediaminetetraacetic acid [EDTA] and 1% [*w*/*v*] triton X-100 with protease inhibitor and phosphatase inhibitor mixture) on ice followed by sonication for 5 min with a 30-s interval and centrifugation at 15,000 rpm for 20 min at 4 °C. The supernatant was retained as triton-soluble fraction. Residual pellet was washed twice in 1% triton lysis buffer and centrifuged at 15,000 rpm for 10 min at 4 °C. The pellet was resuspended in 5 volume of 2% sodium dodecyl sulfate (SDS) lysis buffer (10 mM Tris·HCl [pH 7.4], 150 mM NaCl, 1 mM EDTA, 1% [*v*/*v*] triton X-100 and 2% [*w*/*v*] SDS with protease inhibitor and phosphatase inhibitor mixture) with sonication for 5 min with a 30-s interval and centrifugation at 15,000 rpm for 20 min at room temperature. The supernatant was collected as triton-insoluble fraction. The protein concentration was measured using a bicinchoninic acid (BCA) protein assay kit (23227; Thermo Fisher Scientific, Waltham, MA, USA).

Preparation of recombinant α-synuclein monomers and preformed fibrils

Human α-syn preformed fibrils were generated as previously described (Masuda-Suzukake *et al.*, 2014; Ihse *et al*., 2017; Uemura *et al.*, 2018;) with minor modification. *Escherichia coli* BL21 (DE3) (BioDynamics Laboratory, Tokyo, Japan) were transformed with plasmid pRK172 encoding the human α-syn cDNA sequence and incubated in LB medium. The α-syn expression was induced by 0.1 mM isopropyl β-D-1-thiogalactopyranoside for 4 h. The bacteria were pelleted by centrifugation at 4,000 *g* at 4 °C for 5 min and lysed with repeated freeze and thaw and by sonication. The lysate was clarified by boiling for 5 min, followed by centrifugation at 20,400 *g* at 4 °C for 15 min. The supernatant was subjected to ion exchange using Q sepharose fast flow (GE Healthcare, Little Chalfont, UK), and α-syn was precipitated with 50% (% saturation) ammonium sulfate. Purified α-syn was dialyzed against dialysis buffer (150 mM KCl, 50 mM Tris-HCl, pH 7.5) and cleared by ultracentrifugation at 186,000 *g* at 4 °C for 20 min. The protein concentration was determined using a BCA Protein Assay kit (Thermo Fisher). Purified α-syn was diluted in dialysis buffer containing 0.1% (*w*/*v*) NaN_3 to 7 mg/ml, followed by incubation at 37 °C in a shaking incubator (SI-300C; AS ONE, Osaka, Japan) at 1,000 rpm for 10 days. The α-syn preformed fibril pellet was obtained by ultracentrifugation at 186,000 g at 20 °C for 20 min and stored at −80 °C. Before use, the pellet was dissolved in PBS (2 μg/μl) and sonicated for 5 min.

Western blotting

Described in the supplementary materials.

Native polyacrylamide gel electrophoresis

Western blotting using the native polyacrylamide gel electrophoresis (PAGE) method was performed in accordance with the manual of the NativePAGE™ Novex® Bis-Tris Gel System (MAN0000557; Thermo Fisher). In brief, the samples in the triton-soluble fraction of mouse midbrain (10 μg) or human cortex (20 μg) were mixed with Native PAGE™ Sample Buffer (4×) (BN2003; Thermo Fisher) and Native PAGE™ 5% G-250 Sample Additive (BM2004, Thermo Fisher). The samples were then subjected to a 4–16% Bis-Tris Protein Gel (BN1002BOX, Thermo Fisher) and electrophoresed at a voltage of 150 V at room temperature. During electrophoresis, the cathode buffer was changed from Dark Blue Cathode Buffer (contains 0.02% G-250) to Light Blue Cathode Buffer (contains 0.002% G-250) when the dye front had migrated through about one third of the gel. The samples were transferred to a polyvinylidene difluoride (PVDF) membrane followed by fixation for 30 min at room temperature with 4% (*w*/*v*) paraformaldehyde (PFA) in PBS. The excess Coomassie stain was rinsed for 10 min with 50% (*v*/*v*) methanol. After blocking for 1 h with 5% (*w*/*v*) skim milk in

PBS, the membranes were incubated with anti-α-synuclein primary antibody (listed in supplementary table 2) overnight at 4 °C followed by reaction with horseradish peroxidase-conjugated secondary antibody (1:5000, NB7574; Novus Biologicals, Centennial, CO, USA) for 1 h at room temperature. Immunoreactive bands were detected with detection reagent (02230; Nacalai Tesque, Kyoto, Japan), and the chemiluminescent signal was detected with Amersham Imager 600 (GE Healthcare).

Filter trap assay

A filter trap assay was performed as previously described (Maesako *et al.*, 2012; Wan and Chung, 2012) with some modification. The triton-soluble fraction of mouse midbrain (0.5 μg/μl), α-syn monomer (0.5 ng/ μl) and α-syn preformed fibril (0.5 ng/ μl) were subjected to vacuum filtration through a 96-well microfiltration apparatus (170-6542; Bio-Rad) containing a 200-nm-pore cellulose acetate membrane (11020004; ADVANTEC, Tokyo, Japan). The resultant membrane was fixed for 30 min with 4% (*w*/*v*) PFA in PBS at room temperature. After blocking for 1 h with 5% (*w*/*v*) skim milk in PBS, the membranes were incubated with primary antibodies (listed in supplementary table 2) overnight at 4 °C followed by reaction with horseradish peroxidase-conjugated secondary antibody (1:5000, NB7574; Novus Biologicals) for 1 h at room temperature. Immunoreactive bands were detected with detection reagent

(02230; Nacalai Tesque), and the chemiluminescent signal was detected with Amersham Imager 600 (GE Healthcare).

Behavioral tests

Described in the supplementary materials, except for the details of the olfactory test and sleep analysis.

Electrophysiological recording surgery

A connector/electrode for electroencephalography (EEG) and electromyography (EMG) recordings was implanted into the skull of each mouse. The two pins of the electrode for EEG recording were placed over the right cerebral hemisphere (anterior electrode: 1.26 mm lateral to midline, 0 mm anterior to bregma; posterior electrode: 1.26 mm lateral to midline, 5.0 mm posterior to bregma). The stainless steel wires (AS633; Cooner Wire) of the electrode for EMG recording were inserted bilaterally into the neck muscles of each mouse, and each electrode was attached to the skull using dental cement (56818; 3M, St. Paul, MN, USA). After a one-week recovery period, the animals were moved to a recording cage.

Sleep recording and analyses

For the EEG/EMG recordings, 20- to 55-week-old male mice were used. Cables for signal output were connected to the implanted electrodes, and the animals were allowed to move freely. Signals were amplified through an amplifier (AB-611J; Nihon Koden, Tokyo, Japan) and digitized with an analog-to-digital converter (NI PCIe-6320; National Instruments, Tokyo, Japan) and an appropriate software program (LabView; National Instruments). Animals were allowed at least one week to adapt to the recording conditions prior to any EEG/EMG recording session and handled daily to minimize nonspecific stress. During the EEG/EMG recording, the behaviors of the animals were monitored by cameras to observe their motor activity during sleep. Sleep/wake stages were determined by a visual inspection of the EEG/EMG data in 20-s epochs, as previously described (Funato *et al*., 2016). To determine the "EMG variance" value, we integrated EMG power over 0.5-s bins and calculated the arithmetic variance of EMG power over 8 consecutive 0.5-s bins (over 4-s). The median of 5 consecutive 4-s values of EMG variance was then taken as the EMG variance of each 20-s epoch and used as raw data. We then normalized the REM sleep EMG variance by the same mouse's non-REM (NREM) sleep EMG variance on the same day at the same ZT hour.

Olfactory preference and avoidance test

The olfactory test was performed as previously described (Kobayakawa *et al.*, 2007) with some

modification. In brief, the mice were placed in the test cage (W32.5 cm × D21.5 cm × H13 cm). Two pieces of filter paper (2 cm × 2 cm) were set at the bottom of the cage (8.5 cm from the long side and 6.5 cm from each short side).

For the olfactory preference test, a test odorant was introduced into the filter paper at one side of the cage, and water was introduced into the filter paper at the opposite side of the cage. The sides treated with the odorant and water were changed every test. The sniffing time of the odorant was measured.

For the olfactory avoidance test, a bisector was placed in the cage, and two pieces of filter paper were set on opposite sides of the cage. A test odorant was introduced into the filter paper at one side of the cage, and water was introduced into the filter paper at the opposite side of the cage. The time spent in the opposite area from the odorant-treated filter paper was measured.

Statistical analyses

Statistical significance was evaluated using a one-way factorial analysis of variance (ANOVA) followed by Dunnett's post-hoc test for multiple comparison. Student's *t*-test was used to compare two groups of data. To assess the EEG and EMG data, the non-parametric Mann-Whitney *U* test was implemented. Statistical significance was set at $*P < 0.05$ or $** P < 0.01$.

Date availability

Date are available from the corresponding author on request.

Results

The native expression pattern of human α-syn in the A53T BAC-SNCA transgenic mice

To enhance the aggregation propensity of α-syn, we inserted A53T, rs11931074 (G to T), and rs3857059 (A to G) point mutations as well as the Rep1 copy number variation (259 to 261) into the 190-kb BAC-*SNCA* transgenic construct, which presumably contains the coding sequence as well as gene expression regulatory regions (Fig. 1A). The transgenic line was backcrossed more than 10 generations and maintained on a C57BL/6J background. The transgenic constructs were inserted into the chromosome 9 (Fig. S1). The expression pattern of the transgenic α-syn closely resembled that of the endogenous rodent α-syn (Fig. 1B). When compared with wild-type mice, heterozygous A53T BAC-*SNCA* transgenic (BAC-*SNCA*$^{A53T/-}$) mice expressed 1.5-fold more α-syn, and homozygous A53T BAC-*SNCA* transgenic (BAC-*SNCA*$^{A53T/A53T}$) mice expressed 2.5-fold more α-syn (Fig. 1C and D). In addition, phosphorylated α-syn (p-α-syn) was increased 3.5-fold in BAC-*SNCA*$^{A53T/-}$ mice and 5.5-fold in BAC-*SNCA*$^{A53T/A53T}$ mice (Fig. 1C and E). To avoid potential off-target effects of genomic transgene insertions, we chose BAC-*SNCA*$^{A53T/-}$ mice for further analyses in the present study.

Increased truncated and triton-insoluble α-syn in the BAC-SNCA$^{A53T/-}$ mice

We examined a variety of pathological post-translational modifications of α-syn, including truncation and phosphorylation. Truncated α-syn species enhance α-syn fibril assembly and promote the ability of full-length α-syn to aggregate (Beyer *et al.*, 2013). In the process of α-syn fibril formation, conformational changes of α-syn occur, transforming from soluble oligomers to insoluble fibrils. We conducted an immunoblot analysis in each brain region (olfactory bulb, striatum, midbrain, hippocampus and thalamus) and found that triton-soluble α-syn was increased 1.1- to 3.0-fold in each brain region of BAC-*SNCA*$^{A53T/-}$ mice compared with wild-type mice (Fig. 2A and B), and the amount of oligomeric α-syn was increased in BAC-*SNCA*$^{A53T/-}$ mice in an age-dependent manner (Fig. 2A). The amount of triton-soluble truncated α-syn was increased up to 13-fold in BAC-*SNCA*$^{A53T/-}$ mice (Fig. 2A, C). In addition, BAC-*SNCA*$^{A53T/-}$ mice also showed 1.2- to 6.4-fold more triton-insoluble α-syn in each brain region than wild-type mice (Fig. 2D, E).

Increased proteinase K-resistant α-syn in the BAC-SNCA$^{A53T/-}$ mice

Since abnormally aggregated α-syn in the Lewy bodies is known to be proteinase K (PK)-resistant (Takeda *et al.*, 2000; Tanji *et al.*, 2010), we treated mouse brain sections with PK and

immunostained them with p-α-syn antibody. Whereas PK treatment diminished the immunoreactivity of p-α-syn in the wild-type mouse brains, PK-resistant p-α-syn was still abundant in the BAC-*SNCA*$^{A53T/-}$ mouse brains (Fig. 3A). PK-resistant p-α-syn was highly expressed in the cell body of vulnerable regions in α-synucleinopathy, including the olfactory bulb, anterior olfactory nucleus, deep layer of the cerebral cortex, amygdala, hippocampus, SNc and dorsal motor nucleus of the vagus nerve (DMN). In addition, abundant punctate staining was observed in the olfactory bulb, deep layer of the cerebral cortex and striatum (Fig. 3B), suggesting that α-syn aggregates in nerve terminals. An immunoelectron microscopic study showed that immunogold-labeled p-α-syn existed diffusely in the nucleus and presynaptic regions of neurons of BAC-*SNCA*$^{A53T/-}$ mice. In addition, some clusters of immunogold particles indicating p-α-syn were observed in the presynaptic regions, probably corresponding to the punctate staining of p-α-syn on immunohistochemistry. However, no filamentous structures were observed in the cell bodies or dendrites of p-α-syn–positive neurons (Fig. 3C).

Degeneration of DA neurons in the substantia nigra pars compacta of BAC-SNCA$^{A53T/-}$ mice

DA neuronal loss in the SNc is important pathological feature of Parkinson's disease. We

counted the number of TH-positive neurons in the SNc and found that it was decreased in the BAC-*SNCA*$^{A53T/-}$ mice in an age-dependent manner (Fig. 4A). In contrast, neurons in the ventral tegmental area (VTA) were spared (Fig. S2). When the SNc was divided into four subdivisions according to the morphology, size and distribution of the cell (Fu *et al.*, 2012), the degree of neuronal loss was more severe in the SNcd than in the other subdivisions in the SNc (Fig. S3). Semithin sections with toluidine blue staining revealed atrophic and densely stained neurons in the aged BAC-*SNCA*$^{A53T/-}$ mice, which is suggestive of dark cell degeneration (Fig. 4B), originally reported by Turmaine *et al.* as the pathological finding observed in chronic non-apoptotic neurodegeneration in Huntington disease mice model. (Turmaine *et al.*, 2000). Electron microscopic images showed the accumulation of lipofuscin granules in the neurons of both aged genotypes. However, more atrophic and electron-dense neurons were observed in the BAC-*SNCA*$^{A53T/-}$ mice (Fig. 4C. a-d). The neurons of BAC-*SNCA*$^{A53T/-}$ mice were surrounded by electron-lucent processes, which were considered to be part of the foot processes of adjacent astrocytes (Fig. 4C. e and f) (Ikuta *et al.*, 1983).

Since neuronal degeneration of α-synucleinopathy starts at the synaptic terminals (Calo L *et al.,* 2016), we investigated the TH and dopamine transporter (DAT) expression in the striatum. There was no obvious difference between genotypes on immunoblot analyses (Fig.

S4).

Increased oligomeric α-syn species in the SNc of BAC-SNCA$^{A53T/-}$ mice

α-syn oligomers are widely believed to be involved in DA neuronal degeneration (Mor *et al.,* 2017; Ono K., 2017; Bengoa-Vergniory N *et al*., 2017). To examine α-syn oligomers and fibrils in DA neurons, we performed immunohistochemistry on tissue sections of the substantia nigra in the BAC-*SNCA*$^{A53T/-}$ mice using O1 antibody (specifically reactive with α-syn oligomer and fibril) and F2 antibody (specifically reactive with α-syn fibril) (Vaikath *et al*., 2015). While F2 antibody detected solid structure of Lewy bodies and Lewy neurites, O1 detected fine structures in addition to Lewy bodies and Lewy neurites in the brain of patient with dementia with Lewy bodies (DLB) (Fig. 5A). The SNc sections of wild-type mice were not stained with either antibody, whereas those of BAC-*SNCA*$^{A53T/-}$ mice were punctately stained only with O1 antibody (Fig. 5A). In addition, we conducted native PAGE, which is useful for detecting native protein conformation, and observed high-molecular-weight α-syn in the midbrain of BAC-*SNCA*$^{A53T/-}$ mice in an age-dependent manner (Fig. 5B). In addition, we performed a filter trap assay using a 200-nm-pore cellulose acetate membrane that trapped high-molecular-weight α-syn but not monomeric α-syn and found that triton-soluble oligomeric α-syn in the midbrain

was increased in BAC-*SNCA*$^{A53T/-}$ mice in an age-dependent manner (Fig. 5C and D) Taken together, these results suggested the formation of α-syn oligomers in the SNc of BAC-*SNCA*$^{A53T/-}$ mice. In addition to the SNc, high-molecular-weight α-syn was increased in Parkinson's disease-related regions in the BAC-*SNCA*$^{A53T/-}$ mice (Fig. S5).

RBD-like behavior and hyposmia in BAC-SNCA$^{A53T/-}$ mice

Non-motor symptoms are frequently present before the onset of motor symptoms in Parkinson's disease, and from the perspective of the DMT, they are very important for identifying Parkinson's disease patients in the prodromal stage of the disease (Postuma R B, *et al., 2*012). We conducted a comprehensive battery of behavioral tests to detect motor and non-motor symptoms in BAC-*SNCA*$^{A53T/-}$ mice. First, we examined the motor and cognitive functions using the rotarod test, light and dark transition test, Y-maze test and Barnes maze test. However, we failed to note any marked differences between genotypes in nine-month-old mice (Fig. S6). Next, we examined the non-motor phenotypes, focusing on the RBD-related symptoms and hyposmia. We chose these two phenotypes for our analysis due to their strong association with the future development of Parkinson's disease.

We examined the sleep/wake characteristics of the BAC-*SNCA*$^{A53T/-}$ mice by EEG and

EMG recordings. In wild-type mice (n=5), REM sleep is characterized by sinusoidal theta-frequency EEG activity and absent or minimal EMG activity (Figure 6A and Movie 1). In BAC-*SNCA*$^{A53T/-}$ mice (n=6), we observed excessive muscle twitches in their body and limb during REM sleep (Figure 6A and Movie 2). These abnormal movements during REM sleep in BAC-*SNCA*$^{A53T/-}$ mice were accompanied by transient increases in muscle activity, while wild-type mice showed minimal muscle tone throughout REM sleep (Fig. 6A). We quantified these transient EMG activities by determining the EMG power for every 0.5-s bin and calculating the EMG power variance among the 0.5-s bins over each epoch (see Methods). We scored each epoch as REM sleep only when the delta/theta ratio was below 1.0. Compared with wild-type mice, BAC-*SNCA*$^{A53T/-}$ mice had significantly higher EMG variances during REM sleep at 11 and 13 months of age, although these tendencies were already present at 5 months of age (Fig. 6B). The neck EMG variance during REM sleep in BAC-*SNCA*$^{A53T/-}$ mice was elevated by >180% compared to that during NREM sleep, while this value was approximately 100% in control mice. There was no significant difference in total time and duration of awake/NREM/REM sleep (Fig. S7). These results suggest that these mice experience REM sleep without atonia (RSWA), similar to RBD patients.

Next, we focused on the RBD-related regions (Valencia *et al.*, 2017, 2018; Peever *et*

al., 2014). P-α-syn immunoreactivity was observed in the cell body of the pedunculopontine tegmental nucleus (PPN), sublaterodorsal tegmental nucleus (SLD) and punctate p-α-syn staining was observed in the alpha gigantocellular nucleus (GiA). At younger time-point, these signals were also observed but obscure (Fig. 6C).

We performed the olfactory preference test in nine-month-old male mice. The time spent by BAC-*SNCA*$^{A53T/-}$ mice sniffing female mouse urine was significantly shorter than that of wild-type mice (Fig. 7 A, C and D). In the olfactory avoidance test, the stay time in the hexanone area of BAC-*SNCA*$^{A53T/-}$ mice was longer than that of wild type mice (Fig. 7B, E and F). Taken together, these findings indicate that BAC-*SNCA*$^{A53T/-}$ mice showed hyposmia.

Discussion

Generation of a mouse model for prodromal Parkinson's disease

In recent years, non-motor symptoms have been drawing attention as important prodromal symptoms for Parkinson's disease. Among them, PSG-proven RBD was reported to have the highest conversion rate to Parkinson's disease, and following up patients with RBD non-invasively enables us to obtain valuable information about the disease progression in the premotor stage of Parkinson's disease. However, as the number of patients with PSG-proven RBD is limited, an animal model for prodromal Parkinson's disease has been sought in order to directly trace the symptoms and pathologies in the early or asymptomatic stages of Parkinson's disease. Furthermore, considering that 60%-70% of DA cells are already lost when motor symptoms start in Parkinson's disease, these symptoms are also indispensable in preclinical studies concerning the development of DMTs that need to be started before the emergence of motor symptoms (Fearnley JM *et al*., 1991; Lang AE *et al*., 1998; Dauer W *et al*., 2003).

Based on reports showing that patients with *SNCA* duplication develop Parkinson's disease with prodromal symptoms indistinguishable from idiopathic Parkinson's disease, we created *SNCA* BAC transgenic mice mildly expressing wild-type human α-syn in its natively

expressed regions (Ibáñez P *et al*., 2004; Konno *et al*., 2016). These mice exhibited decreased anxiety-like behaviors but failed to exhibit the motor phenotype and the DA neuronal loss in the SNc (Yamakado *et al*., 2012). Recent genetic studies and GWASs in Parkinson's disease (Satake *et al*., 2009) have shown that risk SNPs and repeat polymorphism in the 5' region (Rep-1) of *SNCA* increase the α-syn expression. We therefore introduced Rep-1 risk polymorphism, two risk SNPs and an A53T mutation into *SNCA*-BAC transgenic construct in order to enhance the α-syn expression and aggregation to create symptomatic mice model for Parkinson's disease. As expected, α-syn is expressed in its natively expressing regions and accumulated in the regions where Lewy pathology is commonly observed in Parkinson's disease.

DA neuronal loss and α-syn oligomer formation

α-syn aggregation and DA neuronal loss in the SNc are pathological hallmarks in Parkinson's disease. PK-resistant phosphorylated as well as truncated α-syn, which are pathological forms of α-syn observed in Parkinson's disease brains, were accumulated in the Parkinson's disease-related regions in BAC-*SNCA*$^{A53T/-}$ mice. However, only a small amount of truncated or insoluble α-syn were observed in the midbrain and morphologically abnormal filamentous α-syn aggregates were not observed even by the electron microscope in BAC-*SNCA*$^{A53T/-}$ mice.

These results raised a question concerning the mechanisms underlying DA cell loss in BAC-*SNCA*$^{A53T/-}$ mice. First, a small amount of truncated or insoluble α-syn in immunoblot might be because the immunoblot was performed against whole part of midbrain, not limited to the SNc, due to the technical difficulties and the same tendency was previously reported in wild-type BAC-*SNCA* trangenic rat (Nuber *et al*., 2013). Second, accumulating evidence has shown that not only α-syn fibrils but also oligomers play a central role in the neuronal degeneration in Parkinson's disease (Winner *et al*., 2011; Martin *et al*., 2012). For instance, soluble and lipid-dependent α-syn oligomers were shown to have accumulated in the brains of patients with Parkinson's disease and dementia with Lewy bodies (DLB) (Sharon *et al*., 2003), and the A53T mutation of α-syn was reported to facilitate its oligomerization *in vitro* (Conway *et al*., 2000). As shown in Figure 5, oligomeric α-syn species were increased in the SNc and presumed to be responsible for the DA cell loss in BAC-*SNCA*$^{A53T/-}$ mice. *In vitro*, α-syn oligomerization was found to increase cell toxicity of α-syn (Outerio *et al*, 2008). For instance, oligomeric α-syn was reported to impair the mitochondrial protein import, leading to mitochondrial dysfunction and the production of aberrant reactive oxygen species (Di Maio *et al*., 2016). *In vivo* study, the elevation of dopamine in A53T α-syn transgenic mice was reported to increase high-angstrom soluble α-syn oligomer, which induced progressive nigrostriatal degeneration and

locomotion disability (Mor *et al.,* 2017). Moreover, it was reported that α-syn oligomerization induced by the dopamine catabolite impaired synaptic vesicles function and lead to neurodegeneration (Plotegher *et al*, 2017). These lines of evidence further support the idea that high-molecular-weight α-syn species (oligomers) detected in the midbrain of the BAC-*SNCA*$^{A53T/-}$ mice may contribute to the loss of DA neurons in the SNc.

In Parkinson's disease patients and α-syn transgenic animals, nigrostriatal degeneration starts at the synapse in the striatum and then retrogradely spreads to the cell body in the SNc (Cheng *et al*., 2010; Rockenstein *et al*., 2014). We examined the presynaptic proteins in DA nerve terminals as well as DA content in the striatum, and found that the expression level of TH and striatal DA content in BAC-*SNCA*$^{A53T/-}$ mice were not markedly different from that of wild-type mice, probably due to the compensatory upregulation of TH protein and DA biosynthesis in the remaining neurons. Similarly, the expression of DAT in BAC-*SNCA*$^{A53T/-}$ mice was not significantly decreased compared to wild-type. Again, this is not inconsistent with the mild DA cell loss in BAC-*SNCA*$^{A53T/-}$ mice, because the expression level of DAT was increased in α-syn overexpression mice (Bellucci *et al*., 2011; Yamakado *et al*., 2012; Mor *et al*., 2017) and decreased in α-syn knockout mice (Bellucci *et al*., 2011; Chadchankar *et al*., 2011; Fountaine *et al*., 2007). α-syn was reported to maintain DAT in the endosomal recycling pathway and to

regulate the cell surface expression (Bellucci *et al*., 2008, 2011).

Motor and non-motor symptoms in BAC-SNCA$^{A53T/-}$ mice

The BAC-*SNCA*$^{A53T/-}$ mice did not show motor symptoms related to Parkinson's disease, which is reasonable, as the number of DA neurons decreased only 17.1% at 18 months of age in BAC-*SNCA*$^{A53T/-}$ mice compared to that in wild-type mice.

In addition to subtle motor changes, non-motor symptoms are important as prodromal symptoms in Parkinson's disease. Among them, PSG-confirmed RBD and hyposmia are particularly important because they have a high conversion rate to Parkinson's disease in the future. Some of the α-syn-based transgenic mice showed hyposmia or sleep disturbance as non-motor symptoms (Fleming *et al*., 2008; Zhang *et al*., 2015; McDowll *et al.*, 2014; Rothman *et al.*, 2013), but RBD-like behaviors were not noted.

In Parkinson's disease, odor detection and discrimination are impaired, even before the actual diagnosis (Goldman JG and Postuma R., 2014). In BAC-*SNCA*$^{A53T/-}$ mice, p-α-syn was accumulated along the main and accessory olfactory pathways, probably contributing to hyposmia; however, we were unable to specify the main lesions responsible for hyposmia. In previous studies, transgenic mice overexpressing α-syn under the *Thy-1* promoter showed

hyposmia (Fleming *et al*., 2008) and displayed PK-resistant α-syn inclusions throughout the olfactory bulb, including in the external portion of the olfactory nucleus, accessory olfactory bulb and glomerular layer of the olfactory bulb, similar to BAC-*SNCA*$^{A53T/-}$ mice. Human A53T α-syn-overexpressing mice under the prion promoter also exhibited hyposmia, accompanied by a decreased number of cholinergic neurons in the mitral cell layer and the decreased activity of acetylcholinesterase in the olfactory bulb (Zhang *et al*., 2015). However, the mechanism underlying hyposmia in Parkinson's disease is complicated, and many factors may contribute to hyposmia. BAC-*SNCA*$^{A53T/-}$ mice are expected to be useful for achieving further insight into the mechanisms involved in hyposmia in Parkinson's disease.

Several studies have explored the regions responsible for RBD. In animal studies, glutamatergic neurons within the SLD in the dorsomedial pons have been shown to activate glycine/GABA inhibitory neurons in the ventromedial medullary reticular formation (VMRF), including the ventral gigantocellular nucleus (GiV), raphe magnus (RMg) and GiA nuclei. During REM sleep, the inhibitory input from these VMRF neurons to spinal motoneurons suppresses muscle tone, and its decreased activity causes RSWA, which is a prerequisite for the diagnosis of RBD. Based on these findings, the neurons in the SLD and VMRF are considered to be the regions responsible for RSWA (Valencia *et al*., 2018). The PPN is also a

candidate region responsible for RBD (Peever *et al.*, 2014; Valencia *et al*., 2017). In human studies incidental Lewy body disease with RBD patients showed Lewy bodies predominantly in the brainstem, including the subcoeruleus complex, which is the equivalent to SLD in mice. (Uchiyama *et al.*,1995; Boeve *et al*., 2007). In addition, using neuromelanin-sensitive imaging, the signal intensity of the locus subcoeruleus in Parkinson's disease with RBD was shown to be more reduced than that in Parkinson's disease without RBD (García-Lorenzo *et al*., 2013). Considering that the VMRF and subcoeruleus complex are known to be the initial regions of Lewy pathology in Parkinson's disease (Jellinger., 2009), they are major candidate regions responsible for RBD in Parkinson's disease.

In terms of mouse models for Parkinson's disease exhibiting sleep abnormalities, wild-type or A53T α-syn transgenic mice under the *Thy-1* promoter showed a decrease in REM sleep or estimated total sleep time (McDowll *et al*., 2014; Rothman *et al*., 2013), but RSWA/RBD-like behavior was not described. The BAC-*SNCA*$^{A53T/-}$ mice described in the present study are the first mouse model for Parkinson's disease to recapitulate RSWA associated with p-α-syn accumulation in related regions, such as the SLD, VMRF and PPN. BAC-*SNCA*$^{A53T/-}$ showed RSWA without any disturbance of the sleep construction. However, they showed a tendency of increased REM sleep in younger age when they didn't show RSWA. It might be the earlier

phenotype of sleep abnormalities followed by RBD in Parkinson's disease.

RBD is an important prodromal symptom with very high conversion rate to α-synucleinopathy in future. However, the prevalence of RBD, especially that of the PSG-confirmed cases, is low in the prodromal stage and is not as high as that of other non-motor symptoms such as hyposmia and constipation, even in the symptomatic stage. In BAC-*SNCA*$^{A53T/-}$ mice REM without atonia (RSWA), a physiological essential component of RBD, can be detected but these mice do not necessarily show overt phenotype such as RBD symptoms in human Parkinson's disease patients. The same is true for prodromal symptoms in human Parkinson's disease in that multiple α-syn pathology observed in various regions such as the olfactory bulb, lower brainstem nuclei and peripheral autonomic nerves do not necessarily become symptomatic in the early stage. From these viewpoints the low prevalence of REM sleep abnormalities in human may partly come from the low sensitivity of detection for RBD-like symptoms. Another possibility is that in Parkinson's disease there are multiple modes of progression in some of which RBD is spared, and RBD is an uncommon symptom more associated with increased α-syn expression.

Regional vulnerability and the mechanism underlying disease initiation in BAC-SNCA$^{A53T/-}$

mice and Parkinson's disease

The accumulation of PK-resistant p-α-syn was mainly observed in the limbic system, cerebral cortex, olfactory bulb and specific brainstem nuclei. Among them, the olfactory bulb and brainstem nuclei, such as the DMN, raphe nuclei and RBD-related nuclei, correspond to the early Lewy pathology lesions in the course of Parkinson's disease. Despite the substantial accumulation of p-α-syn in the limbic system and cerebral cortex, the cognitive function as assessed by Barnes' maze and the fear condition were not impaired, possibly due to regional differences in functional vulnerability to α-syn deposition in Parkinson's disease.

In addition, our study provided insight into the initiation of Parkinson's disease pathology. It is known that multiple prodromal symptoms, such as hyposmia and RBD, whose responsible regions are the olfactory pathway and lower brainstem nuclei, respectively, are frequently observed simultaneously (Aguirre-Mardones C *et al*., 2015). Considering that these two regions are located far away from each other, this is likely caused by the multifocal initiation of pathology, rather than the simultaneous propagation through the nose-to-brain and gut-to-brain pathways. Indeed, pathological studies have shown the frequent simultaneous involvement of subcortical and cortical regions in Parkinson's disease (Jellinger KA., 2009). These findings, along with the fact that BAC-*SNCA*$^{A53T/-}$ mice present with hyposmia and

RSWA, suggest that the enhanced native topographical expression pattern of α-syn contributes to the multifocal pathology in Parkinson's disease.

Conclusion

BAC-*SNCA*$^{A53T/-}$ mice exhibited mild but age-dependent neurodegeneration and non-motor symptoms of Parkinson's disease associated with α-syn pathologies in the regions that are specifically affected in Parkinson's disease and/or DLB. Thus, this mouse model is important as prodromal Parkinson's disease model and can provide insights into the initiation and progression of the disease, especially in the prodromal stage of Parkinson's disease. It may be also useful for the development of DMTs in preclinical studies for Parkinson's disease.

Acknowledgements

We thank Ms. Rie Hikawa, Mr. Ryutaro Tamano and Ms. Miki Nakamura for their technical assistance.

Funding

We gratefully acknowledge grant support from the Ministry of Education, Culture, Sports, Science, and Technology (R.T., Grant-in-Aid for Scientific Research (A), JP18H04041; Grant-

in-Aid for Scientific Research on Innovative Areas, JP17H05698), the Integrated Neurotechnologies for Disease Studies (Brain/MINDS) from Japan Agency for Medical Research and Development, AMED (R.T., JP18dm0207020, M.K., JP18dm0207024), the Japan Science and Technology Agency, CREST (R.T., JP17gm0710011), JSPS KAKENHI (Grant Number JP14616060) and the Mitsubishi foundation (R.T., No. 29125).

Figure Legends

Figure 1. The distribution and expression of human α-syn in A53T BAC-*SNCA* transgenic mice. (A) A schematic representation of the A53T BAC-*SNCA* construct. The construct consists of PAC AF163864 and BAC AC097478 clones and contains the human α-syn gene and its 28-kb 5'- and 50-kb 3'-flanking regions. An A53T mutation, risk-associated single-nucleotide polymorphisms (rs11931074 G<T and rs3857059 A<G) and Rep1 dinucleotide repeat polymorphism (259 to 261 repeats) were introduced into the *SNCA* and *SNCA* promoter region. (B) Representative immunohistochemical staining images of wild-type and BAC-*SNCA*$^{A53T/A53T}$ mouse brains using Syn-1 (human and rodent α-syn) and LB509 (human α-syn) antibody (6 months). Bar indicates 1 mm. (C) Representative Western blot images of whole-brain triton-soluble fraction using syn1 and p-α-syn antibody of wild-type, BAC-*SNCA*$^{A53T/-}$ and BAC-*SNCA*$^{A53T/A53T}$ mice (18 months; n = 3, each). (D) The densitometric evaluation of the total α-syn expression in (C). The expression of α-syn is 1.5-fold higher in BAC-*SNCA*$^{A53T/-}$ and 2.5-fold higher in BAC-*SNCA*$^{A53T/A53T}$ mice than in wild-type mice (E) The densitometric evaluation of p-α-syn expression in (C). The expression of p-α-syn is 3.5-fold higher in BAC-*SNCA*$^{A53T/-}$ mice and 5.5-fold higher in BAC-*SNCA*$^{A53T/A53T}$ mice than in wild-type mice. Vertical bars represent the mean ± SEM. * $P < 0.05$ by Dunnett's multiple comparison test.

Abbreviations are as follows: α-syn, α-synuclein; BAC, bacterial artificial chromosome; Hu + Ro, human + rodent; PAC, P1-derived artificial chromosome; p-α-syn, phosphorylated α-synuclein; *SNCA*$^{A53T/-}$, heterozygous A53T BAC-*SNCA* transgenic mice.

Figure 2. Increased detergent insolubility of α-syn in BAC-*SNCA*$^{A53T/-}$ mice. (A) Representative Western blot images of the triton-soluble fraction of mice brains using Syn-1 antibody (olfactory bulb, cortex, striatum, midbrain, hippocampus, and thalamus; n = 5 for each age group) and human brains (frontal cortex of control and DLB patients). The expression of truncated α-syn is increased in BAC-*SNCA*$^{A53T/-}$ mice and the DLB patient (long-exposure images). The expression of oligomeric α-syn is also increased in BAC-*SNCA*$^{A53T/-}$ mice in an age-dependent manner. The band pattern of BAC-*SNCA*$^{A53T/-}$ mice resembles that of the DLB patient (super-long-exposure images). (B, C) The densitometric evaluation of (A). The expression of α-syn is increased 1.1- to 3.0-fold in BAC-*SNCA*$^{A53T/-}$ mice. The amount of truncated α-syn is increased up to 13-fold in BAC-*SNCA*$^{A53T/-}$ mice. (D) Representative Western blot images of the triton-insoluble fraction of α-syn in mouse brains (olfactory bulb, cortex, striatum, midbrain, hippocampus, and thalamus; n = 5 for each age group) and human brains (control and DLB patients). The expression of triton-insoluble α-syn is increased in

BAC-*SNCA*$^{A53T/-}$ mice and the DLB patient. (E) The densitometric evaluation of (D). The expression of α-syn is increased 1.2- to 6.4-fold in BAC-*SNCA*$^{A53T/-}$ mice. Vertical bars represent the mean ± SEM. *$P < 0.05$, **$P < 0.01$ by t-test between genotypes. Abbreviations are as follows: α-syn, α-synuclein; A53T/-, heterozygous A53T BAC-*SNCA* transgenic mice; Cont, control; DLB, Dementia with Lewy body; wt, wild-type mice.

Figure 3. Increased levels of PK-resistant p-α-syn in the BAC-*SNCA*$^{A53T/-}$ mice. (A) Representative immunohistochemical staining images for p-α-syn with PK pretreatment in brain sections of both genotypes (3 months) in the low-power fields. Bar indicates 500 μm. (B) Representative immunohistochemical staining images for p-α-syn with PK pretreatment in the high-power fields. Bar indicates 20 μm. Lowercase letters indicate enlarged images of pertinent sections in the low-power field images in (A). (C) Representative immunoelectron microscopy images for p-α-syn in the cortex of the older mice (18-22 months). Bars indicate 1 μm except lower left panel, in which bars indicate 2 μm. Diffuse immunogold particles for p-α-syn are observed in the nucleus and presynapse of BAC-*SNCA*$^{A53T/-}$ mouse brains. A cluster of immunogold particles is observed in some of the presynapses in BAC-*SNCA*$^{A53T/-}$ mouse brains (arrows). (D) Representative immunohistochemical staining images for p-α-syn with PK pretreatment in the cortex of the older mice (19 months). Bar indicates 20 μm. Abbreviations

are as follows: AOB, accessory olfactory bulb; Cox (L3-4), layer 3 to 4 of cerebral cortex; dmX, dorsal motor nucleus of the vagus nerve; OB, olfactory bulb; p-α-syn, phosphorylated α-synuclein; PK, proteinase K; SNc, substantia nigra pars compacta; *SNCA*$^{A53T/-}$, heterozygous A53T BAC-*SNCA* transgenic mice; Str, striatum.

Figure 4. Degeneration of DA neurons in the SNc of BAC-*SNCA*$^{A53T/-}$ mice. (A) Representative immunohistochemical staining images for tyrosine hydroxylase (TH) in the SNc of both genotypes (9 months). Bar indicates 500 μm. The number of TH-positive DA neurons in the SNc is decreased in BAC-*SNCA*$^{A53T/-}$ mice in an age-dependent manner (n = 4-6 for each age group, respectively). (B) Representative semi-thin sectioning images of the SNc of both genotypes (22 months). Some neurons in the SNc are atrophic and densely stained with toluidine blue in BAC-*SNCA*$^{A53T/-}$ mice (white arrows). Bar indicates 50 μm. (C) Representative electron microscopic images of brain sections of both genotypes (22 months). Images of (b), (d) and (f) represent enlarged images of (a), (c) and (e), respectively. Lipofuscin granules are observed in the neurons of both genotypes (a–d). In BAC-*SNCA*$^{A53T/-}$ mice, atrophic and electron-dense neurons with vacuolated Golgi appratuses are observed (c and d). The neurons in the BAC-*SNCA*$^{A53T/-}$ mice are surrounded with electron-lucent processes (asterisks) (c–f). Bar indicates 5 μm. Vertical bars represent the mean ±SEM. **P* < 0.05, ***P*

< 0.01 by t-test for the difference between genotypes. Abbreviations are as follows: A, astrocyte; g, Golgi system; SNc, substantia nigra pars compacta; *SNCA*$^{A53T/-}$, heterozygous A53T BAC-*SNCA* transgenic mice.

Figure 5. Increased levels of oligomeric α-syn in the SNc of BAC-*SNCA*$^{A53T/-}$ mice. (A) Representative immunohistochemical staining images using O1 antibody (reactive to both α-syn oligomer and fibril) and F2 antibody (reactive to α-syn fibril) of the SN of both genotypes (18 months) and the frontal lobe of DLB patients. Bar indicates 20 μm (10 μm in insets). Both O1 and F2 antibody detect Lewy bodies and Lewy neurites in DLB. O1-positive punctate staining is observed only in the brains of BAC-*SNCA*$^{A53T/-}$ mice (arrowheads), while F2 is negative in both genotypes. (B) Representative image of native PAGE in the triton-soluble fraction of the midbrain (n = 3 for each age group). The band pattern of aged BAC-*SNCA*$^{A53T/-}$ mice resembles that of DLB. (C) Representative images of the filter trap assay of the triton-soluble fraction of midbrains of both genotypes using syn1 antibody and F2 antibody. (D) The densitometric evaluation of representative images using syn1 antibody of (C) (n = 3-4 for each age group). Vertical bars represent the mean ± SEM. *P < 0.05 by t-test between genotypes. Abbreviations are as follows: α-syn, α-synuclein; Cont, control; DLB, dementia with Lewy bodies; PFF, pre-formed fibril; *SNCA*$^{A53T/-}$, heterozygous A53T BAC-*SNCA* transgenic mice.

FIGURE 6. RBD-like behavior in BAC-*SNCA*$^{A53T/-}$ mice. (A) Typical EEG and EMG findings of wild-type and BAC-*SNCA*$^{A53T/-}$ mice. Arrows denote muscle twitches. (B) The REM/NREM ratio of the EMG variance during REM sleep in each BAC-*SNCA*$^{A53T/-}$ (n = 6) and wild-type (n = 5) mouse. All values are the mean ± SEM. *p < 0.05, **p < 0.01, Mann-Whitney U test. (C) Representative images of p-α-syn immunohistochemical staining in the field related to RBD of both genotypes (9 months) and younger BAC-*SNCA* $^{A53T/-}$ mice (3 months). Bar indicates 20 μm. Abbreviations are as follows: GiA, alpha gigantocellular nucleus; p-α-syn, phosphorylated α-synuclein; PPN, pedunclopontine tegmental nucleus; RBD, rapid eye movement sleep behavior disorder; SLD, sublaterodorsal tegmental nucleus; *SNCA*$^{A53T/-}$, heterozygous A53T BAC-*SNCA* transgenic mice.

Figure 7. Hyposmia in the BAC-*SNCA*$^{A53T/-}$ mice. (A) Olfactory preference test. (C and D) The duration spent sniffing female mouse urine was significantly decreased in BAC-*SNCA*$^{A53T/-}$ mice. (B) Olfactory avoidance test. (E and F) The duration spent on the opposite side from the hexanone was significantly decreased in BAC-*SNCA*$^{A53T/-}$ mice. The olfactory tests were performed in male wild-type (9 months; n = 21) and BAC-*SNCA*$^{A53T/-}$ mice (9 months; n = 23). Vertical bars represent the mean ± SEM. *P < 0.05, **P < 0.01 by t-test between genotypes. Abbreviation are as follows; *SNCA*$^{A53T/-}$, heterozygous A53T BAC-*SNCA* transgenic mice; Wild-type and wt, wild-type mice.

References

Aguirre-Mardones C, Iranzo A, Vilas D, Serradell M, Gaig C, Santamaría J, Tolosa E. Prevalence and timeline of nonmotor symptoms in idiopathic rapid eye movement sleep behavior disorder. J Neurol 2015; 262: 1568-78.

Baekelandt V, Claeys A, Eggermont K, Lauwers E, De Strooper B, Nuttin B*, et al.* Characterization of lentiviral vector-mediated gene transfer in adult mouse brain. Hum Gene Ther 2002; 13(7): 841-53.

Bellucci A, Collo G, Sarnico I, Battistin L, Missale C, Spano P. Alpha-synuclein aggregation and cell death triggered by energy deprivation and dopamine overload are counteracted by D2/D3 receptor activation. J Neurochem 2008; 106(2): 560-77.

Bellucci A, Navarria L, Falari E, Zaltieri M, Bono F, Collo G, *et al*. Redistribution of DAT/α-synuclein complexes visualized by in situ proximity ligation assay in transgenic mice modeling early Parkinson's disease. PLoS one 2011; 6(12): e27959.

Bengoa-Vergniory N, Robert RF, Wada-Martins R, Alegre-Abarrategui J. Alpha-synuclein oligomers: a new hope. Acta Neruopathol. 2017; 134(6): 819-38.

Berg D, Postuma RB, Adler CH, Bloem BR, Chan P, Dubois B, *et al*. MDS research criteria for prodromal Parkinson's disease. Mov Disord 2015; 30(12) 1600-11

Beyer K, Ariza A. alpha-Synuclein posttranslational modification and alternative splicing as a trigger for neurodegeneration. Mol Neurobiol 2013; 47(2): 509-24.

Boeve BF, Dickson DW, Olson EJ, Shepard JW, Silber MH, Ferman TJ, *et al*. Insights into REM sleep behavior disorder pathophysiology in brainstem- predominant Lewy body disease. Sleep Med 2007; 8(1): 60–4.

Calo L, Wegrzynowicz M, Santivañez-Perez J, Grazia Spillantini M. Synaptic failure and α-synuclein. Mov Disord 2016; 31(2): 169-77.

Cannon JR, Geghman KD, Tapias V, Sew T, Dail MK, Li C, *et al*. Expression of human E46K-mutated alpha-synuclein in BAC-transgenic rats replicates early-stage Parkinson's disease features and enhances vulnerability to mitochondrial impairment. Exp Neurol 2013; 240: 44-56.

Chadchankar H, Ihalainen J, Tanila H, Yavich L. Decresed reuptake of dopamine in the dorsal striatum in the absence of α-synuclein. Brain Res 2011; 1382:37-44.

Chartier-Harlin M-C, Kachergus J, Roumier C, Mouroux V, Douay X, Lincoln S*, et al.* α-synuclein locus duplication as a cause of familial Parkinson's disease. The Lancet 2001; 364(9440): 1167-9.

Cheng HC, Ulane CM, Burke RE. Clinical progression in Parkinson disease and the neurobiology of axons. Ann Neurol 2010; 67(6):715–25.

Conway KA, Lee SJ, Rochet JC, Ding TT, Williamson RE, Lansbury PT Jr. Acceleration of oligomerization, not fibrillization, is a shared property of both alpha-synuclein mutations linked to early-onset Parkinson's disease: implications for pathogenesis and therapy. Proc Natl Acad Sci USA 2000; 97(2): 571–6.

Cronin KD, Ge D, Manninger P, Linnertz C, Rossoshek A, Orrison BM, *et al*. Expansion of the Parkinson disease-associated *SNCA*-Rep1 allele upregulates human alpha-synuclein in transgenic mouse brain. Hum Mol Genet 2009; 18(17): 3274-85.

Dauer W, Przedborski S. Parkinson's disease: mechanism and models. Neuron. 2003; 39(6): 889-909.

Di Maio R, Barrett PJ, Hoffman EK, Barrett CW, Zharikov A, Borah A, *et al.* α-Synuclein binds to TOM20 and inhibit mitochondrial protein import in Parkinson's disease. Sci Transl Med 2016; 8(342): 342ra78.

Fearnley JM, Lees AJ. Ageing and Parkinson's disease: substantia nigra regional selectivity. Brain 1991; 114: 2283-301.

Fleming SM, Tetreault NA, Mulligan CK, Hutson CB, Masliah E, Chesselet MF. Olfactory deficits in mice overexpressing human wildtype α-synuclein. Eur J Neurosci 2008; 28(2): 247-56.

Fountaine TM, Wade-Martins R. RNA interference-mediated knockdown of alpha-synuclein human dopaminergic neuroblastoma cells from MPP(+) toxicity and reduces dopamine

transport. J Neurosci. Res. 2007; 85(2):351-63.

Fu Y, Yuan Y, Halliday G, Rusznák Z, Watson C, Paxinos G. A cytoarchitectonic and chemoarchitectonic analysis of the dopamine cell groups in the substantia nigra, ventral tegmental area, and retrorubral field in the mouse. Brain Struct Funct 2012; 217(2): 591-612.

Funato H, Miyoshi C, Fujiyama T, Kanda T, Sato M, Wang Z, *et al.* Forward-genetics analysis of sleep in randomly mutagenized mice. Nature 2016; 539(7629): 378–83.

García-Lorenzo D, Longo-Dos Santos C, Ewenczyk C, Leu-Semenescu S, Gallea C, Quattrocchi G, *et al*. The coeruleus/subcoeruleus complex in rapid eye movement sleep behaviour disorders in Parkinson's disease. Brain 2013; 136(Pt 7): 2120–9.

Giasson BI, Duda JE, Quinn SM, Zhang B, Trojanowski JQ, Lee VM Neuronal alpha-synucleinopathy with severe movement disorder in mice expressing A53T human alpha-synuclein. Neuron 2002; 34(4): 521–33.

Goldman JG and Postuma R. Premotor and nonmotor features of Parkinson's disease. Curr Opin Neurol. 2014; 27: 434-41.

Han W, Liu Y, Mi Y, Zhao J, Liu D, Tian Q. Alpha-synuclein (*SNCA*) polymorphisms and susceptibility to Parkinson's disease: a meta-analysis. Am J Med Genet B Neuropsychiatr Genet 2015; 168B(2): 123-34.

Hansen C, Bjorklund T, Petit GH, Lundblad M, Murmu RP, Brundin P, *et al*. A novel alpha-synuclein-GFP mouse model displays progressive motor impairment, olfactory dysfunction and accumulation of alpha-synuclein-GFP. Neurobiol Dis 2013; 56: 145-55.

Ibáñez P, Bonnet AM, Débarges B, Lohmann E, Tison F, Pollak P, *et al*. Causal relation between α-synuclein gene duplication and familial Parkinson's disease. Lancet. 2004; 364(9440): 1169-71.

Ihse E, Yamakado H, van Wijk XM, Lawrence R, Esko JD, Masliah E. Cellular internalization of alpha-synuclein aggregates by cell surface heparan sulfate depends on aggregate conformation and cell type. Sci Rep 2017;7:9008.

Ikuta F, Yoshida Y, Ohama E, Oyanagi K, Takeda S, Yamazaki K*, et al.* Revised Pathophysiology on BBB Damage: The Edema as an ingeniously Provided Condition for Cell Motility and Lesion Repair. Acta Neuropathol Suppl 1983; 8: 103-10.

Janezic S, Threlfell S, Dodson PD, Dowie MJ, Taylor TN, Potgieter D, *et al*. Deficits in dopaminergic transmission precede neuron loss and dysfunction in a new Parkinson model. Proc Natl Acad Sci U S A 2013; 110(42): E4016-25.

Jellinger KA. A critical evaluation of current staging of alpha-synuclein pathology in Lewy body disorders. Biochim Biophys Acta 2009; 1792(7): 730-40.

Kirik D, Rosenblad C, Burer C, Lundberg C, Johansen TE, Muzyczka N*, et al.* Parkinson-like neurodegeneration induced by targeted overexpression of alpha-synuclein in the nigrostriatal system. J Neurosci 2002; 22(7): 2780-91.

Kobayakawa K, Kobayakawa R, Matsumoto H, Oka Y, Imai T, Ikawa M*, et al.* Innate versus learned odour processing in the mouse olfactory bulb. Nature 2007; 450(7169): 503-8.

Konno T, Ross OA, Puschmann A, Dickson DW, Wszolek ZK. Autosomal dominant Parkinson's disease caused by *SNCA* duplications. Parkisonism Relat Disord. 2016; 1: S1-6.

Kuo YM, Li Z, Jiao Y, Gaborit N, Pani AK, Orrison BM, *et al*. Extensive enteric nervous system abnormalities in mice transgenic for artificial chromosomes containing Parkinson disease-associated alpha-synuclein gene mutations precede central nervous system changes. Hum Mol Genet 2010; 19(9): 1633-50.

Lang AE, Lozano AM. Parkinson's disease. First of two parts. N Engl J Med. 1998; 339(15): 1044-53.

Luk KC, Kehm V, Carroll J, Zhang B, O'Brien P, Trojanowski JQ*, et al.* Pathological α-synuclein transmission initiates Parkinson-like neurodegeneration in nontransgenic mice. Science 2012; 338(6109): 949-53.

Macchi F, Deleersnijder A, Van den Haute C, Munck S, Pottel H, Michiels A*, et al.* High-content analysis of α-synuclein aggregation and cell death in a cellular model of Parkinson's disease. J Neurosci Methods 2016; 261: 117-27.

Maesako M, Uemura K, Kubota M, Kuzuya A, Sasaki K, Hayashida N*, et al.* Exercise is more effective than diet control in preventing high fat diet-induced β-amyloid deposition and memory deficit in amyloid precursor protein transgenic mice. J Biol Chem 2012; 287(27): 23024-33.

Maraganore DM, de Andrade M, Elbaz A, Farrer MJ, Ioannidis JP, Krüger R*, et al.* Collaborative analysis of alpha-synuclein gene promoter variability and Parkinson disease. JAMA 2006; 296(6): 661-70.

Martin ZS, Neugebauer V, Dineley KT, Kayed R, Zhang W, Reese LC, *et al.* α-Synuclein oligomers oppose long-term potentiation and impair memory through a calcineurin-dependent mechanism: relevance to human synucleopathic diseases. J Neurochem 2012; 120(3): 440–52.

Masuda-Suzukake M, Nonaka T, Hosokawa M, Kubo M, Shimozawa A, Akiyama H*, et al.* Pathological alpha-synuclein propagates through neural networks. Acta Neuropathologica Communications 2014; 2(1): 1-12.

Masuda-Suzukake M, Nonaka T, Hosokawa M, Oikawa T, Arai T, Akiyama H*, et al.* Prion-like spreading of pathological α-synuclein in brain. Brain 2013; 136(4): 1128-38.

McDowll KA, Shin D, Roos KP, Chesselet MF. Sleep dysfunction and EEG alterations in mice overexpressing alpha-synuclein. J Parkinsons Dis 2014; 4(3): 531-9.

Mor DE, Tsika E, Mazzulli JR, Gould NS, Kim H, Doshi S *et al.* Dopamine induces soluble α -synuclein oligomers and nigrostriatal degeneration. Nat Neurosci. 2017; 20(11): 1560-8.

Nuber S, Harmuth F, Kohl Z, Adame A, Trejo M, Schonig K, *et al*. A progressive dopaminergic phenotype associated with neurotoxic conversion of alpha-synuclein in BAC-transgenic rats. Brain 2013; 136(Pt 2): 412-32.

Olgiati S, Thomas A, Quadri M, Breedveld GJ, Graafland J, Eussen H*, et al.* Early-onset parkinsonism caused by alpha-synuclein gene triplication: Clinical and genetic findings in a novel family. Parkinsonism & Related Disorders 2015; 21(8): 981-6.

Ono K. The oligomer hypothesis in α-synucleinopathy. Neurochem Res. 2017; 42(12): 3362-71.

Outeiro TF, Putcha P, Tetzlaff JE, Spoelgen R, Koker M, Carvalho F, *et al*. Formation of toxic oligomeric alpha-synuclein species in living cells. PLoS One 2008; 3(4): e1867.

Peever J, Luppi PH, Montplaisir J. Breakdown in REM sleep circuitry underlies REM sleep behaveor disorder. Trends Neurosci 2014; 37(5):279-88.

Plotegher N, Berti G, Ferrari E, Tessari I, Zanetti M, Lunelli L, *et al*. DOPAL derived alpha-synuclein oligomers impair synaptic vesicles physiological function. Sci Rep 2017; 7: 40699.

Poewe W, Seppi K, Tanner CM, Halliday GM, Brundin P, Volkmann J*, et al.* Parkinson disease. Nature Reviews Disease Primers 2017; 3: 17013.

Postuma RB, Aarsland D, Barone P, Burn DJ, Hawkes CH, Oertel W, *et al.* Identifying prodromal Parkinson's disease: pre-motor disorders in Parkinson's disease. Mov Disord 2012; 27(5): 617-26.

Postuma RB, Berg D. Advances in markers of prodromal Parkinson disease. Nat Rev Neurol 2016; 12(11): 622-34.

Rockenstein E, Nuber S, Overk CR, Ubhi K, Mante M, Patrick C, *et al.* Accumulation of oligomer-prone α-synuclein exacerbates synaptic and neuronal degenerateon. Brain 2014; 137(Pt 5): 1496-513.

Rodriguez JA, Ivanova MI, Sawaya MR, Cascio D, Reyes FE, Shi D*, et al.* Structure of the toxic core of α-synuclein from invisible crystals. Nature 2015; 525(7570): 486-90.

Rothman SM, Griffioen KJ, Vranis N, Ladenheim B, Cong WN, Cadet JL, *et al.* Neuronal expression of familial Parkinson's disease A53T α-synuclein causes early motor impairment, reduced anxiety and potential sleep disturbances in mice. J Parkinsons Dis 2013; 3(2):215-9.

Satake W, Nakabayashi Y, Mizuta I, Hirota Y, Ito C, Kubo M*, et al.* Genome-wide association study identifies common variants at four loci as genetic risk factors for Parkinson's disease. Nature genetics 2009; 41(12): 1303-7.

Schapira A, Chaudhuri RK, Jenner P. Non-motor features of Parkinson disease. Nature Reviews Neuroscience 2017; 18(7): 435-50.

Sharon R, Bar-Joseph I, Frosch MP, Walsh DM, Hamilton JA, Selkoe DJ. The formation of highly soluble oligomers of alpha-synuclein is regulated by fatty acids and enhanced in Parkinson's disease. Neuron 2003; 37(4): 583–95.

Spillantini MG, Crowther RA, Jakes R, Hasegawa M, Goedert M. α-Synuclein in filamentous inclusions of Lewy bodies from Parkinson's disease and dementia with Lewy bodies. Proceedings of the National academy of sciences 1998.

Spillantini MG, Schmidt ML, Lee VM, Trojanowski JQ, Jakes R, Goedert M. Alpha-synuclein in Lewy bodies. Nature 1997; 388(6645): 839-40.

Spira PJ, Sharpe DM, Halliday G, Cavanagh J, Nicholson GA. Clinical and pathological features of a Parkinsonian syndrome in a family with an Ala53Thr alpha-synuclein mutation. Ann Neurol 2001; 49(3): 313-9.

Takeda A, Hashimoto M, Mallory M, Sundsumo M, Hansen L, Masliah E. C-terminal alpha-synuclein immunoreactivity in structures other than Lewy bodies in neurodegenerative disorders. Acta neuropathologica 2000; 99(3): 296-304.

Tanji K, Mori F, Mimura J, Itoh K, Kakita A, Takahashi H*, et al.* Proteinase K-resistant α-synuclein is deposited in presynapses in human Lewy body disease and A53T α-synuclein transgenic mice. Acta Neuropathologica 2010; 120(2): 145-54.

Taylor TN, Potgieter D, Anwar S, Senior SL, Janezic S, Threlfell S, *et al*. Region-specific deficits in dopamine, but not norepinephrine, signaling in a novel A30P alpha-synuclein BAC transgenic mouse. Neurobiol Dis 2014; 62: 193-207.

Tran HT, Chung C, Iba M, Zhang B, Trojanowski JQ, Luk KC*, et al.* A-Synuclein immunotherapy blocks uptake and templated propagation of misfolded α-synuclein and neurodegeneration. Cell reports 2014; 7(6): 2054-65.

Turmaine M, Raza A, Mahal A, Mangiarini L, Bates GP, Davies SW. Nonapoptotic neurodegeneration in a transgenic mouse model of Huntington's disease. Proc Natl Acad Sci U

S A 2000; 97(14): 8093-7.

Uchiyama M, Isse K, Tanaka K, Yokota N, Hamamoto H, Aida S, *et al.* Incidental Lewy body disease in a patient with REM sleep behavior disorder. Neurology 1995; 45(4): 709–12.

Uemura N, Yagi H, Uemura MT, Hatanaka Y, Yamakado H, Takahashi R. Inoculation of α-synuclein preformed fibrils into the mouse gastrointestinal tract induces Lewy body-like aggregates in the brainstem via the vagus nerve. Molecular neurodegeneration 2018; 13(1): 21.

Vaikath NN, Majbour NK, Paleologou KE, Ardah MT, van Dam E, van de Berg WD *et al*. Generation and characterization of novel conformation-specific monoclonal antibodies for α -synuclein pathology. Neurobiol Dis. 2015; 79: 81-99.

Valencia Garcia S, Brischoux F, Clément O, Libourel PA, Arthaud S, Lazarus M3, *et al.* Ventromedial medulla inhibitory neuron inactiveation induces REM sleep without atonia and REM sleep behavior disorder. Nat Commun 2018; 9(1): 504.

Valencia Garcia S, Libourel PA, Lazarus M, Grassi D, Luppi PH, Fort P. Genetic inactiveation of glutamate neurons in the rat subletrodorsal tegmental nucleus recapitulates REM sleep behavior disorder. Brain 2017; 140(2):414-28.

Visanji NP, Brotchie JM, Kalia LV, Koprich JB, Tandon A, Watts JC*, et al.* α-Synuclein-Based Animal Models of Parkinson's Disease: Challenges and Opportunities in a New Era. Trends in Neurosciences 2016; 39(11): 750-62.

Wan OW, Chung KKK. The role of alpha-synuclein oligomerization and aggregation in cellular and animal models of Parkinson's disease. PloS one 2012; 7(6).

Wersinger C, Sidhu A. Disruption of the interaction of α-synuclein with microtubules enhances cell surface recruitment for the dopamine transporter. Biochemistry 2005; 44(41): 13612-24.

Winner B, Jappelli R, Maji SK, Desplats PA, Boyer L, Aigner S, *et al. In vivo* demonstration that α-synuclein oligomers are toxic. Proc Natl Acad Sci USA 2011; 108(10): 4194–9.

Yamakado H, Moriwaki Y, Yamasaki N, Miyakawa T, Kurisu J, Uemura K*, et al.* α-Synuclein BAC transgenic mice as a model for Parkinson's disease manifested decreased anxiety-like behavior and hyperlocomotion. Neuroscience Research 2012; 73(2): 173-7.

Zhang S, Xiao Q, Le W. Olfactory dysfunction and neurotransmitter disturbance in olfactory bulb of transgenic mice expressing human A53T mutant alpha-synuclein. PLoS One 2015; 10(3): e0119928.

Figure 1.

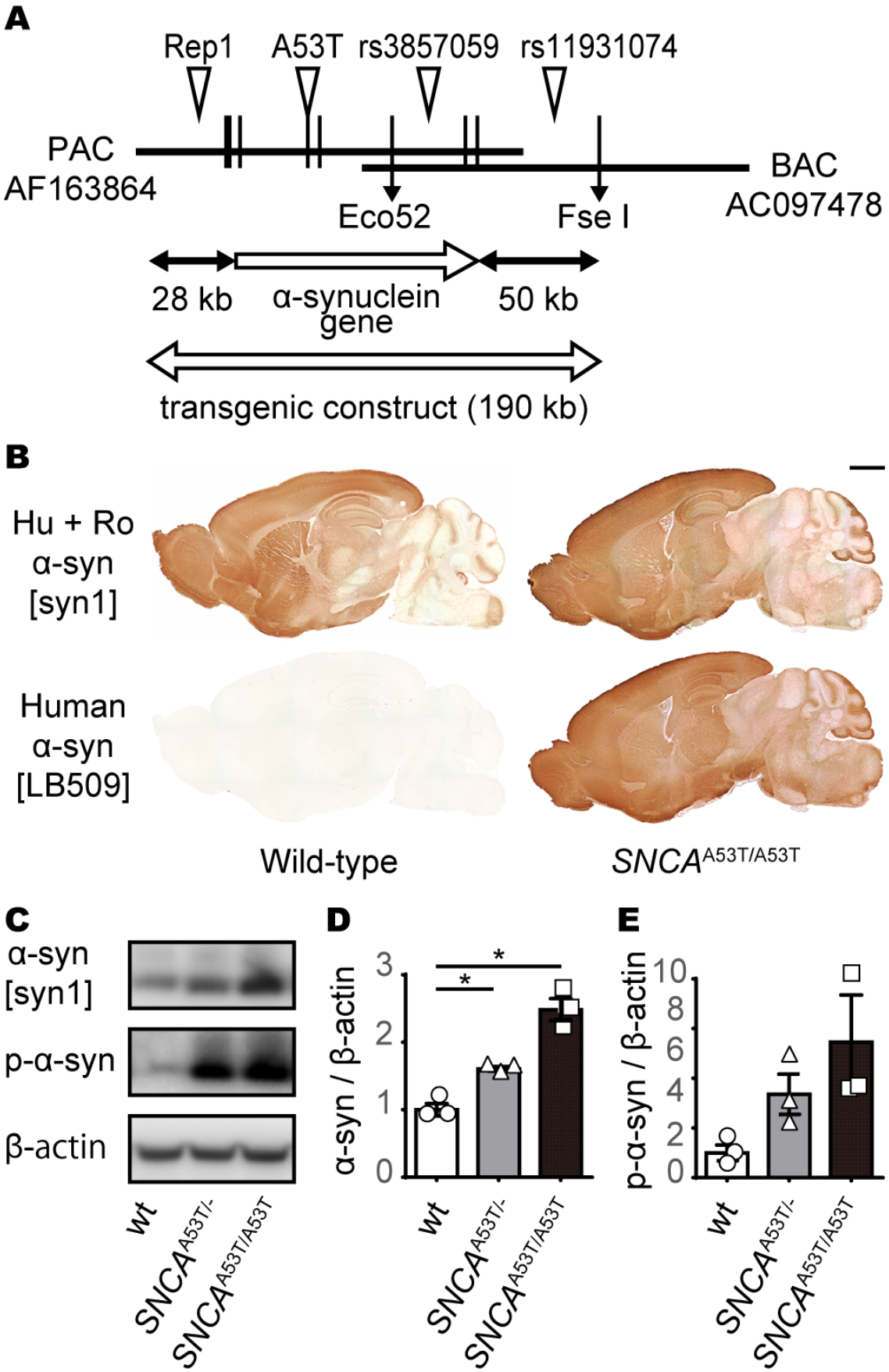
A
Rep1
A53T
rs3857059
rs11931074
PAC
AF163864
BAC
AC097478
Eco52
Fse I
28 kb
α-synuclein gene
50 kb
transgenic construct (190 kb)
B
Hu + Ro α-syn [syn1]
Human α-syn [LB509]
Wild-type
SNCA A53T/A53T
C
α-syn [syn1]
p-α-syn
β-actin
wt
SNCA A53T/-
SNCA A53T/A53T
D
α-syn / β-actin
0
1
2
3
*
*
wt
SNCA A53T/-
SNCA A53T/A53T
E
p-α-syn / β-actin
0
2
4
6
8
10
wt
SNCA A53T/-
SNCA A53T/A53T

Figure 2.

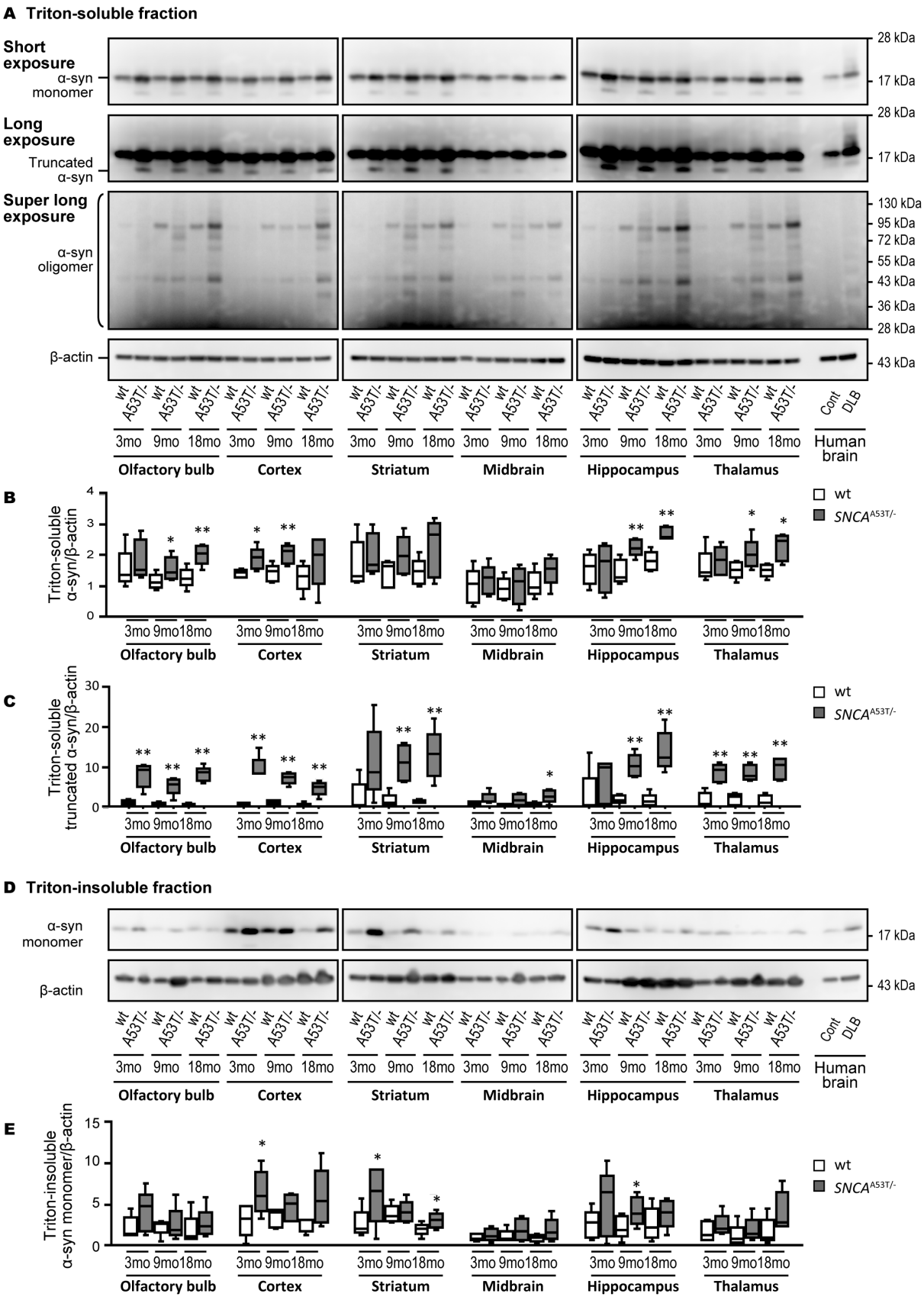
A Triton-soluble fraction
Short exposure
α-syn monomer
Long exposure
Truncated α-syn
Super long exposure
α-syn oligomer
β-actin
28 kDa
17 kDa
130 kDa
95 kDa
72 kDa
55 kDa
43 kDa
36 kDa
wt
A53T/-
Cont
DLB
3mo
9mo
18mo
Human brain
Olfactory bulb
Cortex
Striatum
Midbrain
Hippocampus
Thalamus
B
Triton-soluble α-syn/β-actin
C
Triton-soluble truncated α-syn/β-actin
SNCA A53T/-
D Triton-insoluble fraction
E
Triton-insoluble α-syn monomer/β-actin

Figure 3.

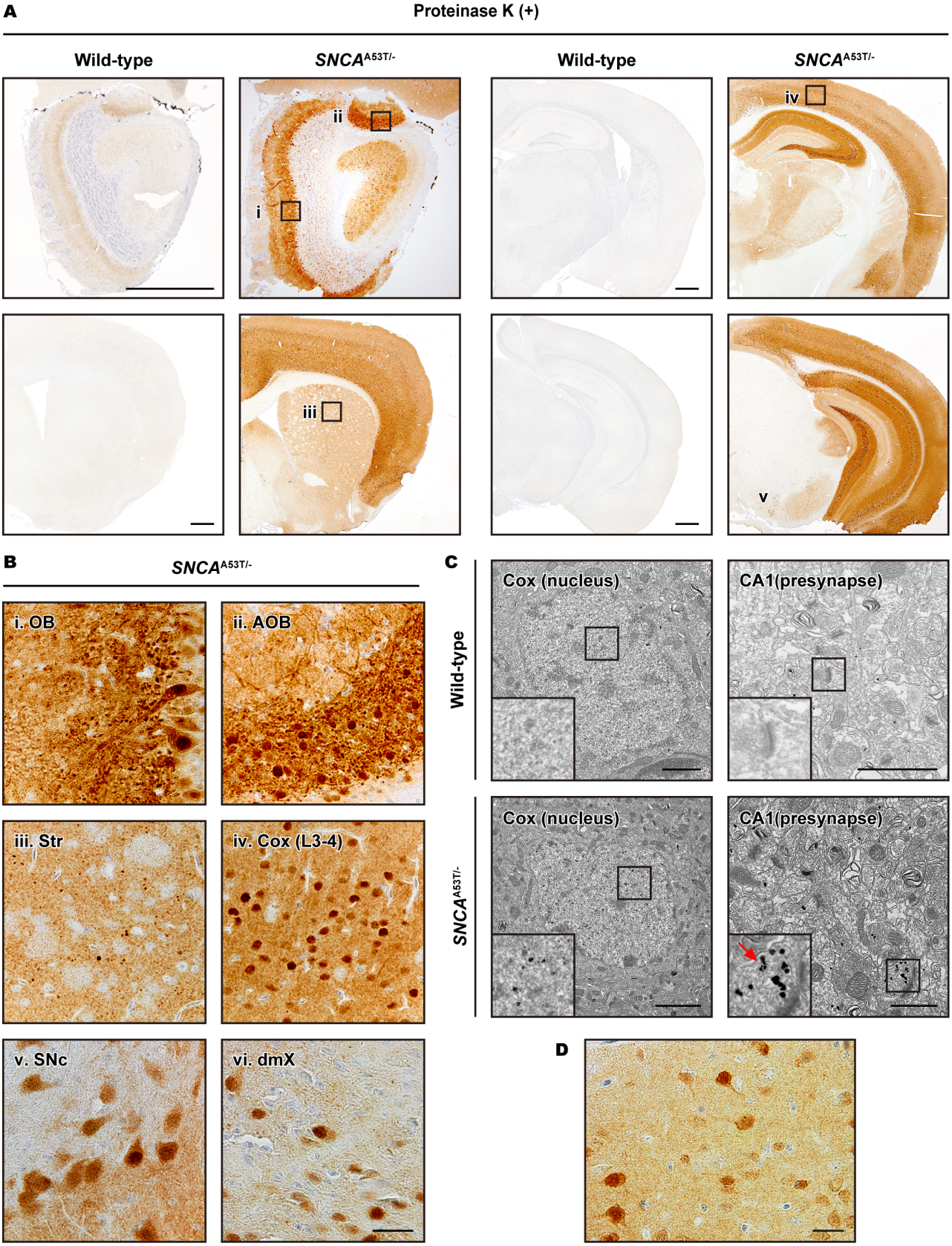
A
Proteinase K (+)
Wild-type
SNCA A53T/-
Wild-type
SNCA A53T/-
i
ii
iii
iv
v
B
SNCA A53T/-
i. OB
ii. AOB
iii. Str
iv. Cox (L3-4)
v. SNc
vi. dmX
C
Wild-type
SNCA A53T/-
Cox (nucleus)
CA1(presynapse)
Cox (nucleus)
CA1(presynapse)
D

Figure 4.

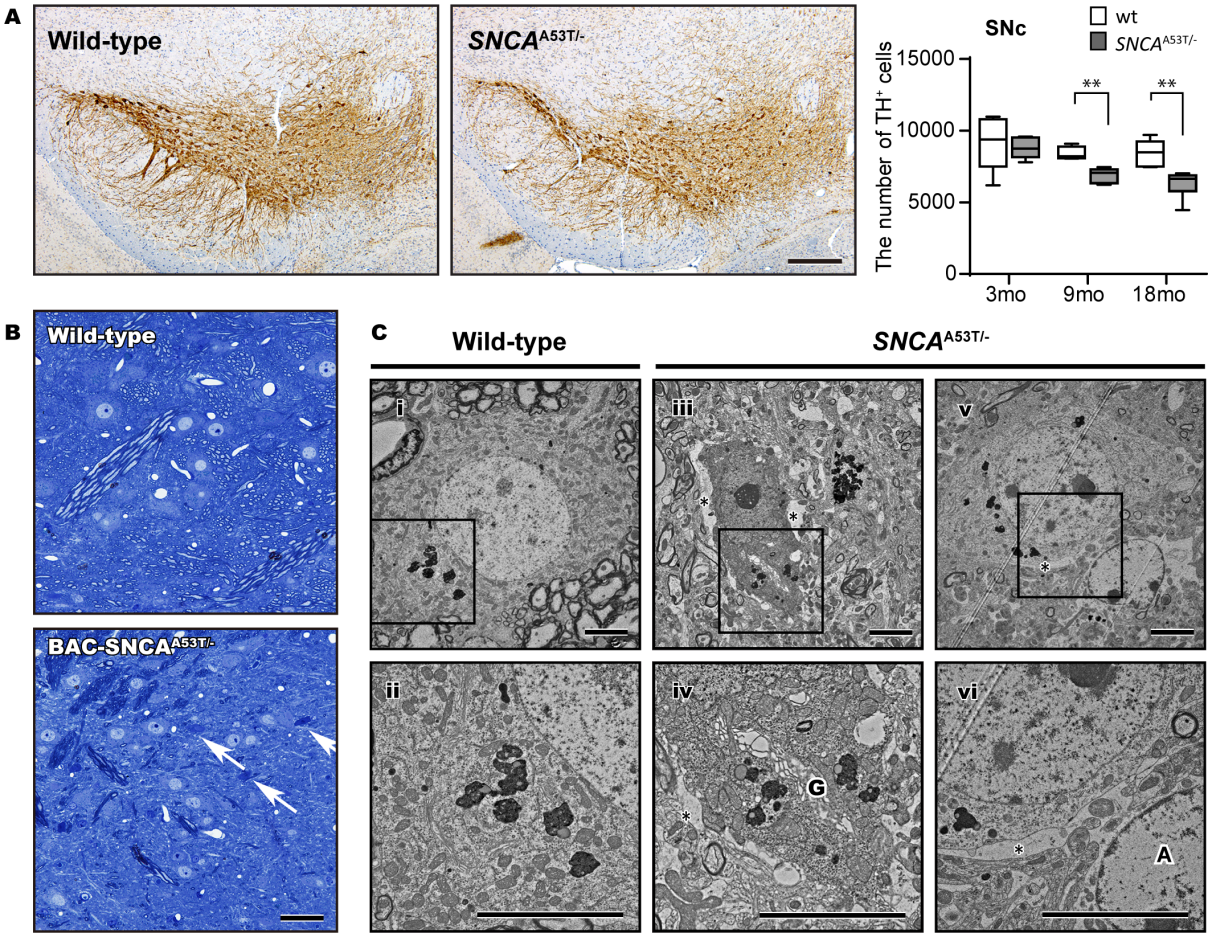
A
Wild-type
SNCA A53T/-
SNc
wt
SNCA A53T/-
The number of TH+ cells
15000
10000
5000
0
3mo
9mo
18mo
**
**
B
Wild-type
BAC-SNCA A53T/-
C
Wild-type
SNCA A53T/-
i
ii
iii
iv
v
vi
G
A

Figure 5.

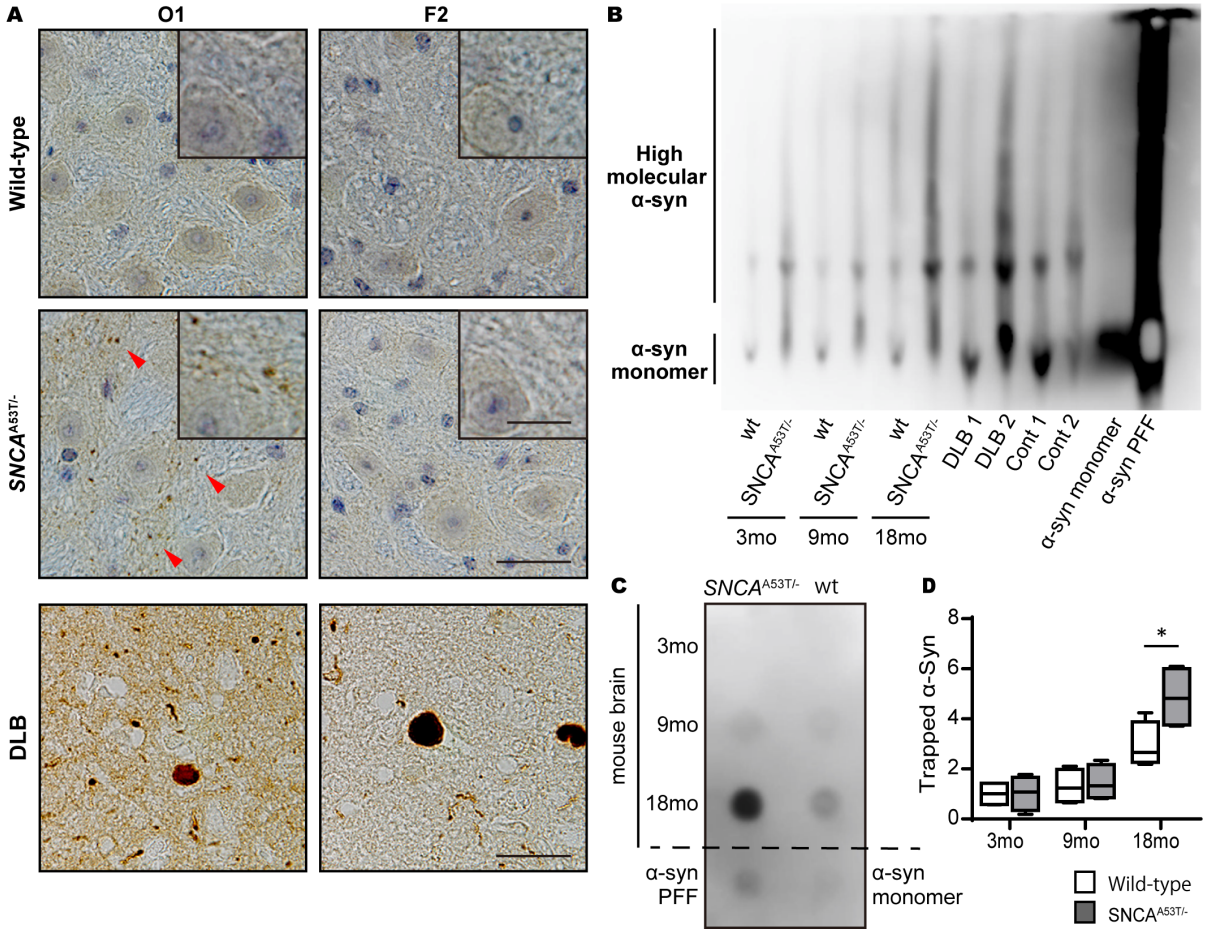
A
O1
F2
Wild-type
SNCA A53T/-
DLB
B
High molecular α-syn
α-syn monomer
wt
SNCA A53T/-
3mo
9mo
18mo
DLB 1
DLB 2
Cont 1
Cont 2
α-syn monomer
α-syn PFF
C
SNCA A53T/-
wt
mouse brain
3mo
9mo
18mo
α-syn PFF
α-syn monomer
D
Trapped α-Syn
Wild-type
SNCA A53T/-

Figure 6.

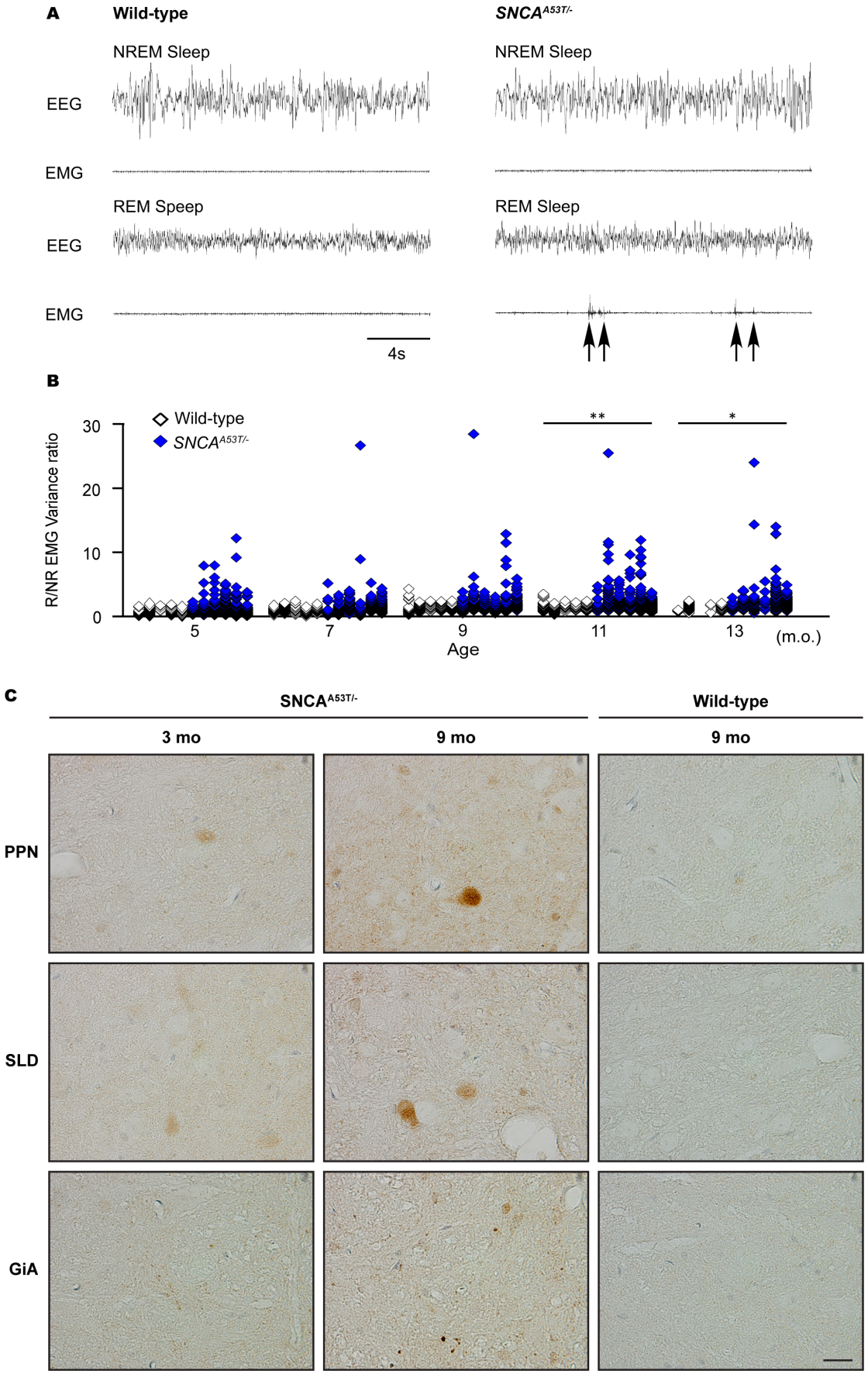
A
Wild-type
SNCA A53T/-
NREM Sleep
EEG
EMG
REM Speep
REM Sleep
4s
B
Wild-type
SNCA A53T/-
R/NR EMG Variance ratio
30
20
10
0
**
*
5
7
9
11
13
(m.o.)
Age
C
SNCA A53T/-
Wild-type
3 mo
9 mo
9 mo
PPN
SLD
GiA

Figure 7.

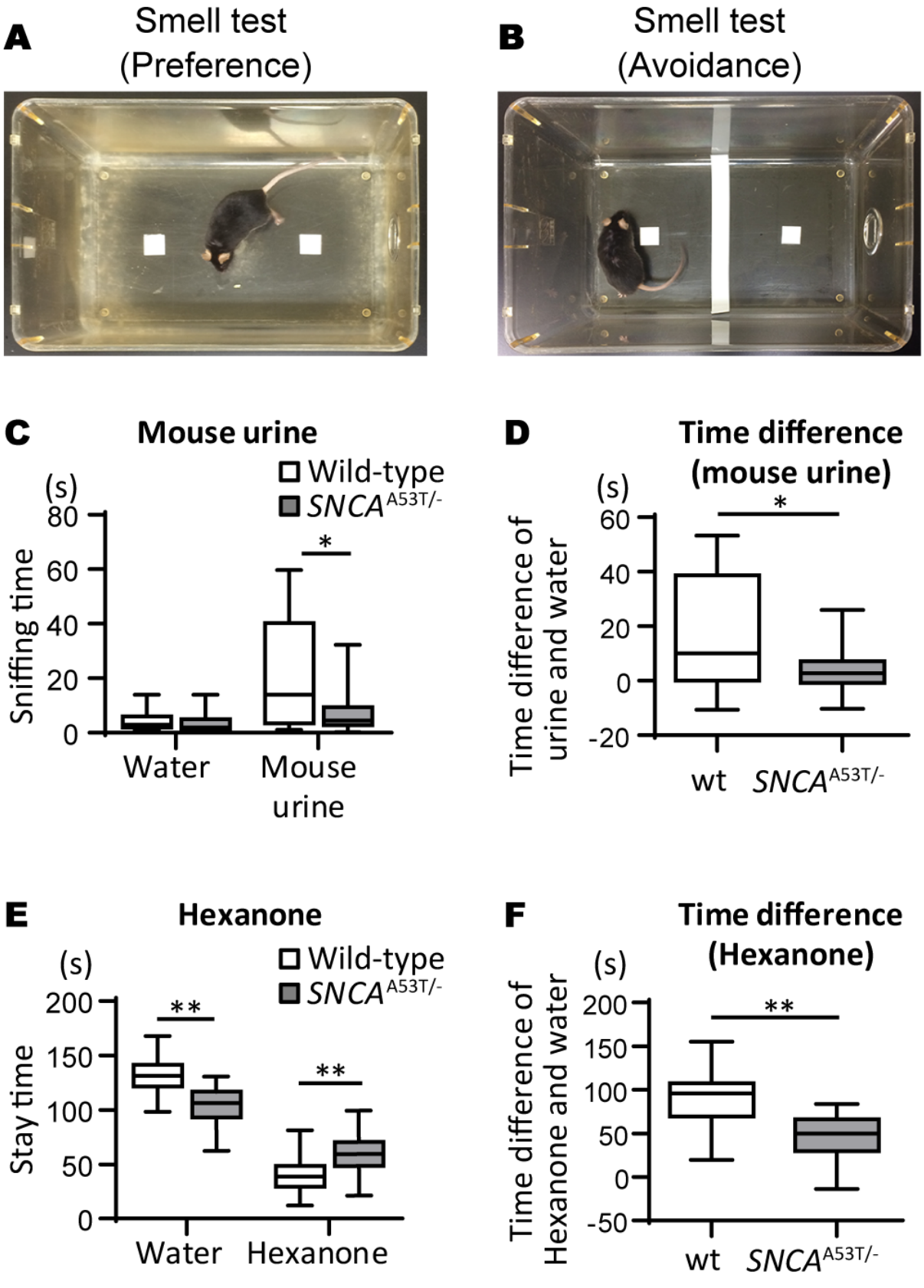
A
Smell test
(Preference)
B
Smell test
(Avoidance)
C
Mouse urine
Wild-type
SNCA A53T/-
(s)
Sniffing time
80
60
40
20
0
*
Water
Mouse urine
D
Time difference
(mouse urine)
(s)
Time difference of urine and water
60
40
20
0
-20
*
wt
SNCA A53T/-
E
Hexanone
Wild-type
SNCA A53T/-
(s)
Stay time
200
150
100
50
0
**
**
Water
Hexanone
F
Time difference
(Hexanone)
(s)
Time difference of Hexanone and water
200
150
100
50
0
-50
**
wt
SNCA A53T/-